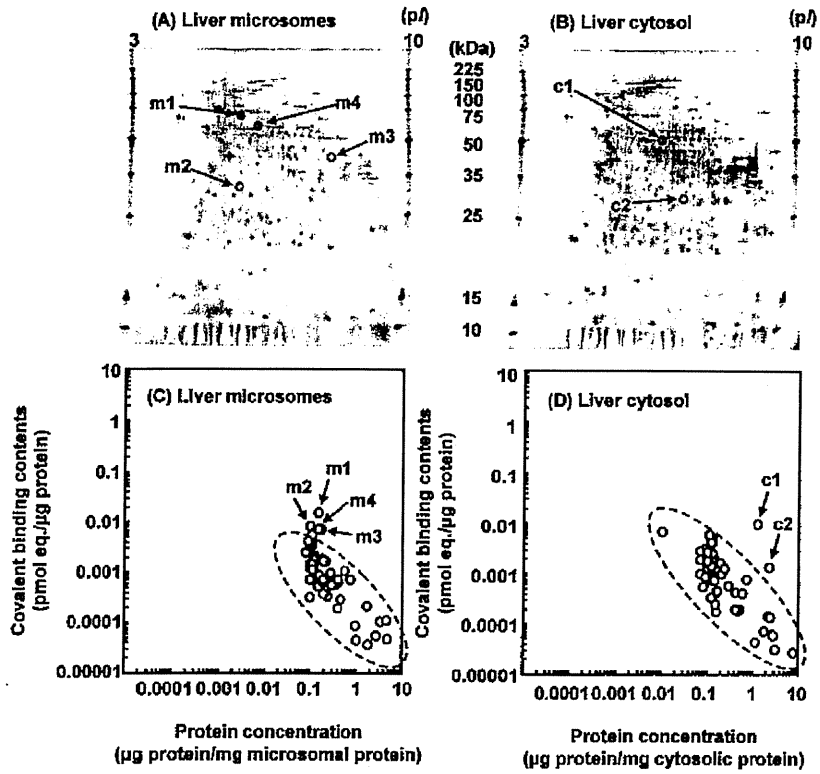


**Figure 6.** Covalent binding profiles of liver microsomal (A,C) and cytosolic (B,D) protein fractions separated by two-dimensional electrophoresis obtained from chimeric mice with humanized liver after the administration of radiolabeled 5-*n*-butyl-pyrazolo[1,5-*a*]pyrimidine (M-5). Loaded protein samples (100 μg) were focused (*x* axis, cathode on the right) and then separated by SDS−PAGE (*y* axis, dye front at bottom) with SYPRO Ruby staining (A,B). *In vivo* protein binding derived from metabolically activated $^{14}$C-5-*n*-butyl-pyrazolo[1,5-*a*]pyrimidine was analyzed by accelerator mass spectrometry (C,D). The typical proteins shown with arrows are m1, prolyl-4-hydroxylase (NCBI accession number gi: 602675); m2, 3-hydroxyanthranic acid dioxygenase (gi: 443919); m3, branched-chain-amino-acid aminotransferase (gi: 2052346); m4, selenium binding protein 1 (acetaminophen binding protein, gi: 16306550); c1, catalase (gi: 4557014); and c2, glutathione *S*-transferase, GSTM2 (gi: 54696748).

to the bioactivated metabolite and was adducted by this to some extent (Figure 5D). The P450 1A2 was separated into fraction 7 in Figure 5B. This fraction 7 on the gel also had P450 2C9 and other proteins with the apparent specific binding of ~2 pmol equiv/mg protein. It would be speculated that the bioactivated 5-*n*-butyl-pyrazolo[1,5-*a*]pyrimidine by P450 1A2 in humanized liver might bind P450 1A2 itself extensively and other surrounding abundant P450 forms or any proteins nonselectively. These P450 forms were not evaluated in two-dimensional electrophoresis because of technical reasons: the membrane-bound proteins were generally difficult to resolve by the first pI-dependent separation step in two-dimensional electrophoresis. However, relatively high specific covalent binding (~2 pmol equiv/μg protein) in the 35−100 kDa proteins (Figure 5) was detected when compared with that of any spots separated in two-dimensional electrophoresis (Figure 6). The drug−protein adducts of bioactivated 5-*n*-butyl-pyrazolo[1,5-*a*]pyrimidine were likely to nonselectively bind any abundant proteins in microsomal or cytosolic proteins shown in Figure 6C and D. Estimated specific bindings (pmol drug equiv/μg protein) apparently indicated an inverse correlation with the protein contents. One of the identified adducted targets was microsomal prolyl-4-hydroxylase, a key enzyme in the biosynthesis of collagens, or an cytosolic antioxidant enzyme catalase that catalyzes the decomposition of hydrogen peroxide to water and oxygen. These lines of evidence strongly suggest that 5-*n*-butyl-pyrazolo[1,5-*a*]pyrimidine, the primary metabolite of a hepatotoxic previous drug candidate for humans, could be bioactivated by human P450 1A2 in humanized liver *in vivo* and would bind any proteins either in microsomes or cytosol including the catalysis of P450 1A2 itself. It could be proposed that covalent binding of drugs via reactive quinone-imine derivatives might show relatively low specificities in target protein bindings.

In conclusion, the hepatotoxic proximate compound 5-*n*-butyl-pyrazolo[1,5-*a*]pyrimidine was activated by human liver microsomal P450 1A2 to reactive intermediate(s) *in vivo* in humanized chimeric mice and could relatively nonspecifically bind to biomolecules such as P450 1A2 and others. Chimeric mice with a human or rat livers would be good predictors to see idiosyncratic drug toxicity *in vivo* in preclinical studies.

**Acknowledgment.** This work was supported in part by the Ministry of Education, Science, Sports and Culture of Japan. We thank Drs. Norie Murayama and Makiko Shimizu for their assistance.

## References

(1) Guengerich, F. P. (2008) Cytochrome P450 and chemical toxicology. *Chem. Res. Toxicol. 21*, 70–83.

(2) James, L. P., Mayeux, P. R., and Hinson, J. A. (2003) Acetaminophen-induced hepatotoxicity. *Drug Metab. Dispos. 31*, 1499–1506.

(3) Kassahun, K., Pearson, P. G., Tang, W., McIntosh, I., Leung, K., Elmore, C., Dean, D., Wang, R., Doss, G., and Baillie, T. A. (2001) Studies on the metabolism of troglitazone to reactive intermediates in vitro and in vivo. Evidence for novel biotransformation pathways involving quinone methide formation and thiazolidinedione ring scission. *Chem. Res. Toxicol. 14*, 62–70.

(4) Gonzalez, F. J., and Yu, A. M. (2006) Cytochrome P450 and xenobiotic receptor humanized mice. *Annu. Rev. Pharmacol. Toxicol. 46*, 41–64.

(5) Kuribayashi, S., Goto, K., Naito, S., Kamataki, T., and Yamazaki, H. (2009) Human cytochrome P450 1A2 involvement in the formation of reactive metabolites from a species-specific hepatotoxic pyrazolopyrimidine derivative, 5-n-butyl-7-(3,4,5-trimethoxybenzoylamino)pyrazolo[1,5-*a*]pyrimidine. *Chem. Res. Toxicol. 22*, 323–331.

(6) Powley, M. W., Frederick, C. B., Sistare, F. D., and DeGeorge, J. J. (2009) Safety assessment of drug metabolites: implications of regulatory guidance and potential application of genetically engineered mouse models that express human P450s. *Chem. Res. Toxicol. 22*, 257–262.
(7) Tateno, C., Yoshizane, Y., Saito, N., Kataoka, M., Utoh, R., Yamasaki, C., Tachibana, A., Soeno, Y., Asahina, K., Hino, H., Asahara, T., Yokoi, T., Furukawa, T., and Yoshizato, K. (2004) Near completely humanized liver in mice shows human-type metabolic responses to drugs. *Am. J. Pathol. 165*, 901–912.
(8) Katoh, M., Tateno, C., Yoshizato, K., and Yokoi, T. (2008) Chimeric mice with humanized liver. *Toxicology 246*, 9–17.
(9) Emoto, K., Tateno, C., Hino, H., Amano, H., Imaoka, Y., Asahina, K., Asahara, T., and Yoshizato, K. (2005) Efficient *in vivo* xenogeneic retroviral vector-mediated gene transduction into human hepatocytes. *Hum. Gene Ther. 16*, 1168–1174.
(10) Inoue, T., Sugihara, K., Ohshita, H., Horie, T., Kitamura, S., and Ohta, S. (2009) Prediction of human disposition toward *S*-$^{3}$H-warfarin using chimeric mice with humanized liver. *Drug Metab. Pharmacokinet. 24*, 153–160.
(11) Laemmli, U. K. (1970) Cleavage of structural proteins during the assembly of the head of bacteriophage T4. *Nature 227*, 680–685.
(12) Sanchez, J. C., Rouge, V., Pisteur, M., Ravier, F., Tonella, L., Moosmayer, M., Wilkins, M. R., and Hochstrasser, D. F. (1997) Improved and simplified in-gel sample application using reswelling of dry immobilized pH gradients. *Electrophoresis 18*, 324–327.
(13) Rabilloud, T., Valette, C., and Lawrence, J. J. (1994) Sample application by in-gel rehydration improves the resolution of two-dimensional electrophoresis with immobilized pH gradients in the first dimension. *Electrophoresis 15*, 1552–1558.
(14) Lopez, M. F., Berggren, K., Chernokalskaya, E., Lazarev, A., Robinson, M., and Patton, W. F. (2000) A comparison of silver stain and SYPRO Ruby Protein Gel Stain with respect to protein detection in two-dimensional gels and identification by peptide mass profiling. *Electrophoresis 21*, 3673–3683.
(15) Kristensen, D. B., Imamura, K., Miyamoto, Y., and Yoshizato, K. (2000) Mass spectrometric approaches for the characterization of proteins on a hybrid quadrupole time-of-flight (Q-TOF) mass spectrometer. *Electrophoresis 21*, 430–439.
(16) Gharahdaghi, F., Weinberg, C. R., Meagher, D. A., Imai, B. S., and Mische, S. M. (1999) Mass spectrometric identification of proteins from silver-stained polyacrylamide gel: a method for the removal of silver ions to enhance sensitivity. *Electrophoresis 20*, 601–605.
(17) Miyaoka, T., Isono, Y., Setani, K., Sakai, K., Yamada, I., Sato, Y., Gunji, S., and Matsui, T. (2007) Bioanalysis works in the IAA AMS facility: Comparison of AMS analytical method with LSC method in human mass balance study. *Nucl. Instrum. Methods Phys. Res., Sect. B 259*, 779–785.
(18) Park, B. K., Kitteringham, N. R., Powell, H., and Pirmohamed, M. (2000) Advances in molecular toxicology-towards understanding idiosyncratic drug toxicity. *Toxicology 153*, 39–60.
(19) Uetrecht, J. (2003) Screening for the potential of a drug candidate to cause idiosyncratic drug reactions. *Drug Discovery Today 8*, 832–837.
(20) Evans, D. C., Watt, A. P., Nicoll-Griffith, D. A., and Baillie, T. A. (2004) Drug-protein adducts: An industry perspective on minimizing the potential for drug bioactivation in drug discovery and development. *Chem. Res. Toxicol. 17*, 3–16.

TX900323A

J Med Dent Sci 2012; 59: 43–52

Original Article

# Hepatic stellate cells mediate differentiation of dendritic cells from monocytes

Rie Ozeki[1], Sei Kakinuma[2], Kinji Asahina[1,*], Keiko Shimizu-Saito[1], Shigeki Arii[2], Yujiro Tanaka[2] and Hirobumi Teraoka[1]

*1) Department of Pathological Biochemistry, Medical Research Institute, Tokyo Medical and Dental University, 2-3-10 Kandasurugadai, Chiyoda-ku, Tokyo 101-0062, Japan*
*2) Graduate School of Medical and Dental Sciences, Tokyo Medical and Dental University, 1-5-45 Yushima, Bunkyo-ku, Tokyo 113-8519, Japan*
**) Present address: Department of Pathology, Keck School of Medicine, University of Southern California, Los Angeles, USA*

***Background*** We have previously reported that human umbilical cord blood (UCB)-nucleated cells differentiate into hepatocyte-like cells when cultured in a 5-cytokine cocktail medium. We further found that UCB cells rather differentiated into dendritic-shaped cells by coculture with a human stellate cell (HSC) line, LI90.
***Methods*** Monocytes from UCB and adult peripheral blood were cocultured with LI90 or rat primary HSCs in a cell-culture insert. Monocytes were also cultured with LI90-conditioned medium containing secreted factors, which were analyzed by a cytokine array.
***Results*** In the coculture with LI90, resulting dendritic-shaped cells from monocytes expressed dendritic cell (DC) markers and activated allogeneic T cells, indicating that the dendritic-shaped cells were DCs. LI90 in the cytokine cocktail medium secreted various inflammatory factors, such as granulocyte-macrophage colony-stimulating factor (GM-CSF) and interleukin-4. Fibroblast growth factor-2 in the cytokine cocktail was responsible for GM-CSF production from LI90 cells and for differentiation of monocytes into DCs in the LI90 coculture. Moreover, the coculture of monocytes with activated HSCs derived from damaged rat liver induced the differentiation of DCs, whereas quiescent HSCs derived from normal liver scarcely induced such a change.
***Conclusion*** These results suggest that activated HSCs are involved in differentiation of monocytes into DCs in the liver.

Key words: hepatic stellate cell, dendritic cell, GM-CSF, FGF-2, the space of Disse

## Introduction

In systemic immune system, dendritic cells (DCs) are the most potent antigen-presenting cells and appear to be the major cell type capable of initiating a primary T cell-dependent immune response.[1] Immature DCs are highly specialized antigen-capturing cells characterized by high expression of CD1a and mannose receptors involved in antigen uptake and phagocytosis.[2] Immature DCs reside in most tissues and are recruited to inflamed sites. After capturing and processing antigens, DCs migrate to the T-cell areas of secondary lymphoid organs and stimulate naïve T cells. In *in vitro* experiments, differentiation of DCs from monocytes is recapitulated in the presence of granulocyte-macrophage colony-stimulating factor (GM-CSF) and interleukin (IL)-4.[3,4] Tumor necrosis factor (TNF)-$\alpha$ and prostaglandin $E_2$ ($PGE_2$) further induce the maturation step of DCs and expression of CD80, CD83 and CD86 *in vitro*.[5,6]

The liver is continuously exposed to a wide range of antigens carried by portal blood from the intestine. In the liver, DCs reside in the sinusoids[7] and play a pivotal

Corresponding Author: Hirobumi Teraoka PhD,
Graduate School of Medical and Dental Sciences, Tokyo Medical and Dental University, Tokyo, 113-8519, Japan.
Tel: +81-3-5803-5811 Fax: +81-3-5803-0212
E-mail: hteraoka.pbc@mri.tmd.ac.jp
Received October 12 : Accepted November 11, 2011

role not only in immune responses but also in tolerance against antigens.[8] Thus, clarifying the recruitment and function of hepatic DCs is critical to understanding the hepatic immune system. The antigen-capturing DCs in the liver are derived from the bone marrow and presumably enter the lymphatic capillaries in the portal area and translocate into the hepatic lymph nodes.[9,10] Cabillic et al.[11] reported that the hepatic environment influences monocyte differentiation into DCs. Although Kupffer cells are known to contribute to recruitment of DCs in the liver,[12] it remains elusive how differentiation, recruitment and translocation of DCs are regulated by different types of liver cells.

Hepatic stellate cells (HSCs) store vitamin A droplets in their cytoplasm and reside in the space of Disse.[13] HSCs secrete hepatocyte growth factor (HGF) and pleiotrophin and induce proliferation of hepatocytes during liver regeneration.[14] Upon liver injury, HSCs are activated and participate in the progression of liver fibrosis.[15,16] The activated HSCs lose their vitamin A storage capacity; express $\alpha$-smooth muscle actin (SMA); secrete cytokines such as fibroblast growth factors (FGFs); and participate in the remodeling of extracellular matrices. HSCs regulate inflammation by secretion of chemokines, including monocyte chemotactic protein (MCP)-1 and macrophage inflammatory protein 2.[17] In addition, HSCs serve as liver-resident antigen-presenting cells.[18] However, it is not known whether HSCs influence immune responses via DCs during liver injury.

We have previously reported that human umbilical cord blood (UCB)-nucleated cells differentiate into hepatocyte-like cells when cultured in a cytokine cocktail medium containing FGF-1, FGF-2, leukemia inhibitory factor (LIF), stem cell factor (SCF) and HGF.[19] During the course of the study, we found that UCB cells rather differentiated into DC-like cells by coculture with a human HSC line, LI90. To test whether HSCs regulate differentiation of DCs in the liver, we further clarified mechanism of HSC-dependent differentiation of DCs from monocytes. In the present study, we found that HSC-induced DC-like cells are functional and that the cultured LI90 cells and activated primary HSCs secrete several cytokines and induce differentiation of DCs from monocytes. These results suggest that HSCs participate in immune responses via induction of DCs during the liver injury.

## Materials and Methods

### Coculture of UCB or peripheral blood cells with LI90

UCB samples from full-term deliveries were collected after informed consent in writing. The study protocol was approved by the ethical committees of Medical Research Institute, Tokyo Medical and Dental University and Kanto Medical Center NTT East Corporation. Adult peripheral blood was obtained from healthy volunteers after informed consent in writing. Nucleated cells in the UCB samples were obtained using 6% hydroxyethyl starch (Nipro Co., Osaka, Japan) as previously described.[19] To obtain mononuclear cells from UCB or peripheral blood, blood samples were diluted with phosphate buffered saline (PBS) containing 2% bovine serum albumin and 0.6% citrate and layered on top of a Lymphoprep™ (Nycomed, Oslo, Norway). Mononuclear cells were isolated by density centrifugation, and monocytes were obtained by adhesion selection.[20] Human UCB cells were also purchased from RIKEN Bioresource Center (Tsukuba, Japan). UCB cells ($2 \times 10^7$ cells/well) or monocytes ($5 \times 10^6$ cells/well) were cultured in a 6-well plate (Becton Dickinson, Franklin Lakes, NJ, USA) coated with 0.1% gelatin in Dulbecco's modified Eagle's medium (Sigma, St. Louis, MO, USA) supplemented with 15% fetal bovine serum (JRH Biosciences, Lenexa, KS, USA), 2 mM L-glutamine, 25 mM HEPES, 100 U/ml penicillin, 100 $\mu$g/ml streptomycin, 0.25 mg/ml amphotericin B, and 300 $\mu$M monothioglycerol (DMEM/FBS medium) at 37°C in a 5% $CO_2$ atmosphere. The culture medium was supplemented with human recombinant cytokines including 20 ng/ml FGF-1 (Invitrogen, Grand Island, NY, USA), 10 ng/ml FGF-2 (Invitrogen), 10 ng/ml LIF (Chemicon, Temecula, CA, USA), 10 ng/ml SCF (R&D Systems, Minneapolis, MN, USA) and 10 ng/ml HGF (a kind gift from Mitsubishi Chemical Co., Tokyo, Japan). An LI90 cell line was kindly provided by Dr. T. Matsuura (The Jikei University School of Medicine, Tokyo, Japan).[21] LI90 was seeded on the membrane of cell culture insert (Becton Dickinson) that is composed of transparent polyethylene terephthalate membrane (0.45 $\mu$m). The LI90 in the insert was cocultured with UCB or peripheral blood cells on the 6-well plates up to day 21. For maturation of DCs, the culture continued in the medium supplemented with 1 ng/ml $PGE_2$ (Sigma) and 25 ng/ml TNF-$\alpha$ (Invitrogen) for additional 2 days. The conditioned medium was collected 7, 14 and 21 days after culture of LI90 with the 5-cytokine cocktail upon

medium changes at day 7 and 14. Peripheral blood monocytes were cultured in LI90-conditioned medium containing 1 μg/ml anti-human GM-CSF antibody (R&D Systems) or control IgG for 21 days. At day 7 and 14, a half medium was changed to the fresh medium.

### RT-PCR

Total RNA was extracted using an RNeasy Kit (Qiagen, Tokyo, Japan). cDNAs were synthesized with 100 ng total RNA by using Superscript II and oligo (dT) primers (Invitrogen) according to the manufacturer's instruction. The resulting cDNA was amplified with AmpliTaq Gold (Applied Biosystems, Branchburg, NJ, USA) under the following conditions: for human glyceraldehyde 3-phosphate dehydrogenase (Gapdh) (5'-TGAAGGTGCGTGTGAACGGATTTGGC, 5'-TGTTGGGGGCCGAGTTGGGATA), at 95°C for 4 min followed by 30 cycles at 95°C for 30 sec, 60°C for 30 sec and 72°C for 25 sec; for human CD83 (5'-TCAAGTTATTGGAGGGTGGTG, 5'-GAGAAAAGCTCGTTCCATGC), at 95°C for 4 min followed by 33 cycles at 95°C for 30 sec, 60°C for 30 sec and 72°C for 25 sec; for human DC derived C-C chemokine (DC-CK1) (5'-GCCAGGTGTCATCCTCCTAA, 5'-GGCACAATGTCTGCTGAGAA), at 95°C for 4 min followed by 35 cycles at 95°C for 30 sec, 55°C for 30 sec and 72°C for 30 sec. For rat Gapdh (5'-CCAATGTATCCGTTGTGGAT, 5'-GTCTGGGATGGAATTGTGAG) at 95°C for 4 min followed by 25 cycles at 95°C for 30 sec, 58°C for 30 sec and 72°C for 30 sec; for rat GM-CSF (5'-GCTCACCCAACCCTGTCAC, 5'-CTCATTTCTGGACCGGCTTC) at 95°C for 4 min followed by 35 cycles at 95°C for 30 sec, 62°C for 30 sec and 72°C for 30 sec. The amplified PCR products were separated by electrophoresis on 1.5% agarose gels and stained with ethidium bromide.

### Immunocytochemistry

The cultured UCB cells were fixed with 80% acetone at -20°C for 10 min and washed three times with PBS. Endogenous peroxidase was inactivated with 3% $H_2O_2$. The cells were incubated for 1 h with anti-human α-SMA monoclonal antibody conjugated with horseradish peroxidase (DAKO EPOS kit; clone 1A4, DAKO, Kyoto, Japan), and then washed three times with PBS. The signal was detected using 3,3'-diaminobenzidine tetrahydrochloride (DAB) liquid system (DAKO) according to the manufacturer's instruction. For analysis of CD83, the cells were incubated for 1 h with anti-human CD83 antibody conjugated with FITC (1:50; clone HB15e, Ancell, Bayport, MN, USA). The cells were washed three times with PBS and observed under a fluorescence microscope. The cells were fixed with 4% paraformaldehyde/PBS at room temperature for 20min and washed three times with PBS. Then they were blocked with 5% donkey serum containing 0.2% bovine serum albumin at room temperature for 30min and washed three times with PBS. The cells were incubated for 1 h with anti-human CD83 antibody (1:100; clone HB15e, R&D system) or anti-human DC-SIGN (CD209) antibody (1:100; R&D system). Then the cells were incubated with mouse IgG conjugated with Alexa-Fluor 488.

### Mixed leukocyte reaction

Allogeneic mixed leukocyte reaction was performed as previously described.[22] T cells were isolated from adult mononuclear cells by a T cell negative isolation kit according to the manufacturer's instruction (DYNAL, Oslo, Norway). Allogeneic adult T cells (1 x $10^5$ responder cells/well) were cultured in triplicate in flat-bottom 96-well plates (Greiner, Nutingen, Germany) with different number of stimulator cells (DC: T cell ratio of 1:320-1:5) pretreated with mitomycin-C. Cultures were maintained in RPMI-1640 (Sigma) supplemented with 10% FBS. To the well containing 200 μl medium, 20 μl of 100 μM 5'-bromo-2'-deoxyuridine (BrdU) was added 18 h before the end of a 5-day culture, and its incorporation was then determined with BrdU kit (Roche Diagnostics, Mannheim, Germany).

### Cytokine array

Human cytokine array membranes were purchased from RayBiotech, Inc. (Norcross, GA, USA). Human cytokine array 3 was used according to the manufacturer's direction. We assayed 42 cytokines in conditioned medium that was collected after LI90 cells cultured with or without the cytokine cocktail for 21 days.

### Enzyme-linked immunosorbent assay (ELISA) for GM-CSF

Measurement of GM-CSF in the medium of LI90 culture was performed by using AN'ALYZA Immunoassay System (GT, Minneapolis, MN, USA) as the manufacturer's protocol. LI90 cells were cultured in 6-well plates at a density of 4 x $10^4$ cells/well for 21 days in the several culture systems. Medium was changed at day 7 and 14. Supernatants were collected at day 7, 14 and 21 of culture. Determination of GM-CSF concentration was performed in triplicate.

### Coculture of UCB cells with primary HSCs

Male Wistar rats (220-300g body weight) were used. All experiments were performed according to the standard guidelines for animal experiments of the Tokyo Medical and Dental University. Rats were subjected to intraperitoneal injection of 1.5 ml $CCl_4$/kg body weight (Wako Pure Chemical Industries, Osaka, Japan).[23] HSCs were isolated from normal or $CCl_4$-damaged livers.[24] Briefly, normal or damaged livers were perfused for 10 min with SC-1 solution consisting of 8 mg/ml NaCl, 0.4 mg/ml KCl, 0.088 mg/ml $NaH_2PO_4 \cdot 2H_2O$, 0.12 mg/ml $Na_2HPO_4$, 2.38 mg/ml Hepes, 0.35 mg/ml $NaHCO_3$, 0.19 mg/ml EGTA and 0.9 mg/ml glucose (pH 7.3), followed by digestion at 37°C for 40 min with 0.1% pronase E (Merck, Whitehouse Station, NJ, USA) and 0.04% collagenase (Wako Pure Chemical Industries) dissolved in SC-1 solution containing 0.56 mg/ml $CaCl_2 \cdot 2H_2O$ instead of 0.19 mg/ml EGTA and 0.9 mg/ml glucose (SC-2 solution). The digested liver was excised, cut into small pieces, and incubated in SC-2 solution containing 0.08% pronase E, 0.08% collagenase and 20 μg/ml DNase I (Roche). The resulting suspension was filtered through a 150-μm steel mesh and centrifuged on an 8.2% Nycodenz™ (Axis-Shield, Oslo, Norway) cushion, which produced an HSC-enriched fraction in the upper whitish layer. The cells were washed, suspended in DMEM supplemented with 10% FBS, 70 μg/ml penicillin, and 100 μg/ml streptomycin, and plated on plastic culture dishes. Cell purity was approximately 95% as assessed by a typical star-like configuration and by detecting vitamin A autofluorescence. The resulting cells were cocultured with UCB monocytes as described above.

## Results

### Dendritic-shaped cells in coculture with a human HSC line

We previously reported that UCB cells differentiate into hepatocyte-like cells *in vitro*.[19] To test whether HSCs further contribute to hepatic differentiation of UCB cells, we cocultured UCB cells with the human HSC line LI90 using a cell-culture insert in a medium supplemented with the hepatocyte-inducing cytokines containing FGF-1, FGF-2, LIF, SCF and HGF as illustrated in Fig. 1A. Contrary to our expectation, LI90 did not induce hepatocyte-like cells from UCB cells. Instead, dendritic-shaped cells emerged in the UCB cell population10 days after the coculture. At 21 days of culture, these cells comprised approximately 80% of the adherent UCB cell population (Fig. 1B,C). No round-shaped hepatocyte-like cells were observed under the applied coculture conditions; however, these cells were generated from the UCB cells without LI90 coculture (Fig. 1D) as previously reported.[19] Next, we tested whether monocytes isolated from UCB cells are the source of dendritic-shaped cells. When UCB monocytes were cocultured with LI90 cells on a separate insert, dendritic-shaped cells were similarly generated (Fig. 1E). The differentiation into dendritic-shaped cells was

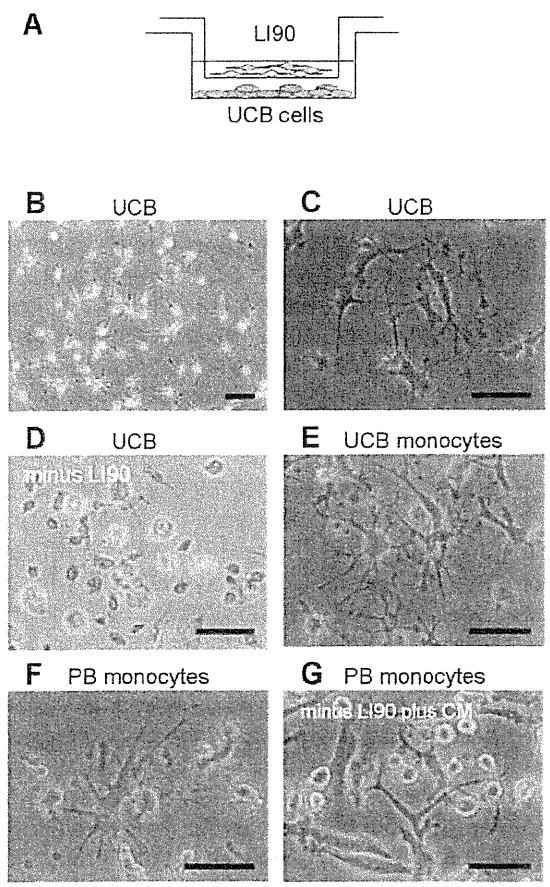


**Figure 1 : Coculture of UCB and peripheral blood cells with a human stellate cell line, LI90.** (A) Coculture system of UCB cells with LI90 cells. LI90 cells were seeded on the membrane of cell culture insert, and human UCB-nucleated cells were seeded on the plastic well in the cytokine cocktail medium containing FGF-1, FGF-2, LIF, SCF and HGF. (B-D) Morphology of UCB-nucleated cells cocultured with (B, C) or without LI90 cells (D) in the cytokine medium for 21 days. Round-shaped cells appeared in (D). (E, F) Morphology of monocytes from UCB (UCB monocytes, E) or peripheral blood (PB monocytes, F) cocultured with LI90 in the cytokine medium for 21 days. (G) Morphology of PB monocytes cultured in the LI90 conditioned medium obtained at 14 days (CM) for 21 days. Scale bars: 100 μm (B, D), 50 μm (C, E-G).

also observed in monocytes isolated from adult peripheral blood in a coculture with LI90 (Fig. 1F). Furthermore, peripheral blood monocytes cultured in a conditioned medium of LI90 cells with the same cytokine cocktail showed morphological changes identical to those in the case of coculture mentioned above (Fig. 1G). These data show that monocytes from UCB and peripheral blood differentiated into dendritic-shaped cells in the presence of factor(s) secreted by LI90 cells in the coculture.

### Characterization of dendritic-shaped cells from UCB cells cocultured with LI90 cells

We characterized whether the UCB-derived dendritic-shaped cells are functionally equivalent to DCs. LI90 cells were immunocytochemically positive for $\alpha$-SMA, a marker of activated HSCs (Fig. 2A). The monocyte-derived dendritic-shaped cells were negative for $\alpha$-SMA (Fig. 2B), but positive for CD83 and DC-SIGN (CD209) (Fig. 2C). RT-PCR revealed no expression of a DC-specific chemokine, DC-CK1 (CCL18),[25] in freshly isolated UCB monocytes (Fig. 2D, day 0). Upon coculturing with LI90, the UCB monocytes commence to express DC-CK1 from day 1 and the expression level gradually increased thereafter (Fig. 2D). No induction of DC-CK1 expression was seen in the UCB monocytes without LI90 coculture (data not shown). These results suggest that monocyte-derived cells induced by LI90 exhibited a DC phenotype *in vitro*.

### Functional analysis of UCB-derived DCs

Next, we tested whether UCB-derived cells stimulate proliferation of T cell, a major function of DCs. After coculturing the UCB monocytes with LI90 for 21 days, the monocyte-derived cells were further cocultured with 1 x $10^5$ T cells obtained from allogeneic peripheral blood and the proliferative activity of the T cells was measured by determining BrdU uptake on day 5. As shown in Fig. 2E (open circle), the monocyte-derived cells induced by LI90 coculture were capable of stimulating T-cell proliferation. The stimulating capacity was as high as that of dendritic-shaped cells cultured with TNF-$\alpha$ and $PGE_2$ for additional 2 days (Fig. 2E, closed circle). These results suggest that LI90 induces functional DCs from monocytes in the coculture condition.

### Identification of factors secreted from LI90 cells in the cytokine medium

Our results indicated that factor(s) secreted by LI90 are responsible for the differentiation of monocytes into the DC lineage in the cytokine cocktail medium. In order to identify these factor(s), we examined the factors present in the LI90 conditioned medium with and without cytokine cocktail using the Human Cytokine Protein Array System. Table 1 presents the ratio of

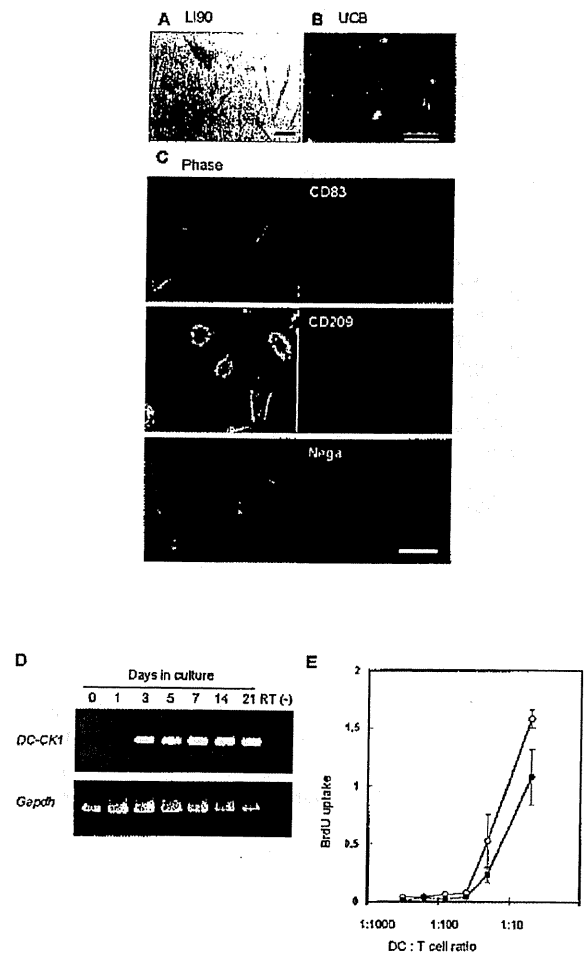


**Figure 2 : Characterization of dendritic-shaped cells derived from UCB cells cocultured with LI90 cells.** Immunostaining of LI90 cells (A) and UCB-derived dendritic-shaped cells (B) with anti-$\alpha$-SMA antibody. Scale bars, 50 $\mu$m. (C) Immunofluorescent staining of dendritic-shaped cells with anti-CD83 or anti-CD209 antibodies. Scale bars, 50 $\mu$m. (D) RT-PCR analysis of DC-CK1 expression in dendritic-shaped cells. The RNA samples were prepared from the cultured UCB monocytes for the indicated days. No amplification was detected in a negative control (Day 21, RT-). Gapdh was used as an internal control. (E) Mixed leukocyte reaction. UCB monocytes were cocultured with LI90 for 21 days, then cultured with (closed circle) or without (open circle) 1 ng/ml $PGE_2$ and 25 ng/ml TNF-$\alpha$ for additional 2 days. The cultured cells ($3.1 \times 10^3$-$2 \times 10^4$ cells) were mixed with 1 x $10^5$ T cells. Cell proliferation was detected by BrdU uptake.

Table 1 : Levels of cytokines in the medium of LI90 cultured with cytokine cocktail.

| fold[a] | cytokine | ratio | fold | cytokine | ratio |
|---|---|---|---|---|---|
| | GM-CSF | 49.195 | | IL-8 | 1.337 |
| | IL-1α | 9.050 | | IL-10 | 1.148 |
| | IL-1β | 109.425 | | IL-12 | 2.217 |
| >5 | IL-4 | 5.305 | | Leptin | 1.226 |
| | IL-13 | 7.125 | 1-5 | MCP-3 | 2.052 |
| | IL-15 | 46.125 | | OSM | 1.182 |
| | MCP-2 | 11.792 | | SCF | 4.068 |
| | Ang[b] | 3.298 | | SDF-1 | 1.731 |
| | EGF | 1.400 | | TARC | 1.204 |
| | ENA-78 | 3.625 | | TNF-α | 1.235 |
| | GCSF | 1.492 | | TNF-β | 1.691 |
| | GRO | 1.911 | | VEGF | 1.453 |
| | GRO-α | 2.418 | | MCP-1 | 0.953 |
| | I-309 | 1.150 | | MCSF | 0.447 |
| 1-5 | IFN-γ | 3.473 | | MDC | 0.134 |
| | IGF-1 | 1.152 | <1 | MIG | 0.094 |
| | IL-2 | 1.736 | | MIP-1δ | 0.134 |
| | IL-3 | 1.622 | | PDGF-β | 0.997 |
| | IL-5 | 2.548 | | RANTES | 0.614 |
| | IL-6 | 1.410 | | TGF-β | 0.843 |
| | IL-7 | 1.709 | | Tpo | 0.990 |

[a] Conditioned medium of LI90 without cytokine cocktails as a control. [b] Ang, angiotensin; EGF, epidermal growth factor; ENA, epithelial neutrophil-activating protein; GCSF, granulocyte-colony stimulating factor; GRO, growth-regulated oncogene; IFN-γ, interferon-γ; IGF-1, insulin-like growth factor-1; OSM, oncostatin M; SDF, stromal cell-derived factor; TARC, thymus and activation-regulated chemokine; VEGF, vascular endothelial growth factor; MCSF, macrophage-colony stimulating factor; MDC, macrophage-derived chemokine; MIG, monokine induced by gamma interferon; MIP-1δ, macrophage inflammatory protein-1δ; PDGF-β, platelet-derived growth factor-β; RANTES, regulated upon activation, normal T-cell expressed, and presumably secreted; TGF-β, transforming growth factor-β; Tpo, thrombopoietin.

cytokine production in the LI90 culture with the cytokine cocktail to without cytokine cocktail. Among the 42 cytokines assayed on the membrane, the production of 7 cytokines, including GM-CSF, IL-1α, IL-1β, IL-4, IL-13, IL-15 and MCP-2, showed more than 5-fold greater increase in the LI90 conditioned medium prepared with the cytokine cocktail medium. In particular, GM-CSF expression was drastically higher (49-fold) in the LI90 cells cultured in the cytokine medium. Since GM-CSF is known as an essential factor for inducing DC differentiation from monocytes,[3,4] we further investigated whether LI90-secreted GM-CSF directly participate DC differentiation from monocytes. When monocytes were cultured in LI90 conditioned medium with a neutralizing antibody against GM-CSF,

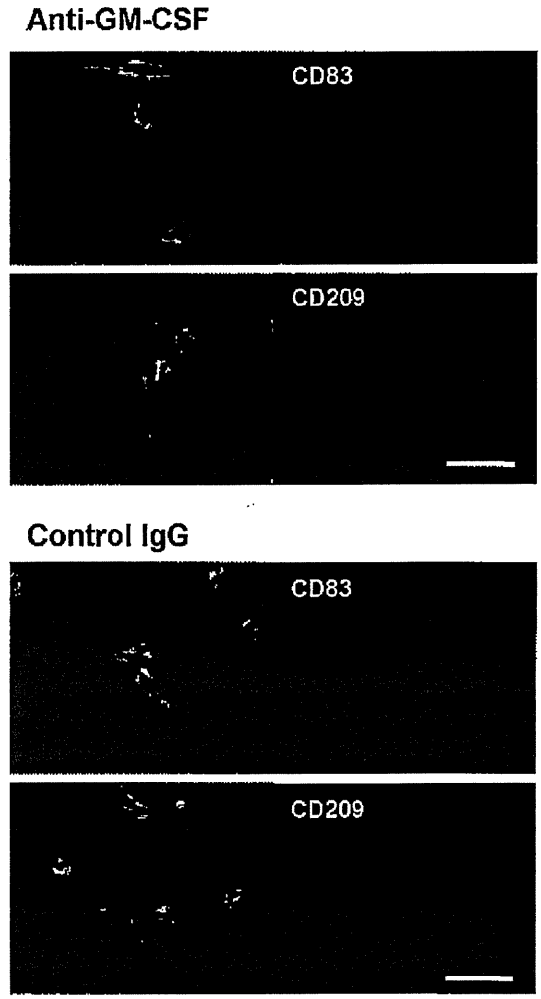


Figure 3 : Suppression of DC induction by anti-GM-CSF antibody. Monocytes from peripheral blood were cultured in the LI90 conditioned medium with anti-GM-CSF antibody or control IgG for 21 days. Immunostaining was carried out using anti-CD83 and anti-CD209 antibodies. The anti-GM-CSF antibody suppresses the expression of CD83 and DC-SIGN (CD209). Scale bars, 50 μm.

they did not change their morphology to dendritic-shaped and no induction of DC markers such as CD83 and CD209 were observed (Fig. 3). The control IgG did not suppress the expression of DC markers. Thus, GM-CSF secreted from LI90 is critical for induction of DCs from monocytes.

### FGF-2 induces GM-CSF secretion in LI90

We measured the time-dependent secretion of GM-CSF from LI90 cells in the presence of the cytokine cocktail by ELISA. The concentration of GM-CSF in the

LI90-conditioned medium was 2.5 ng/ml at 14 days, and increased to 7.8 ng/ml at 21 days (Fig. 4A). On the other hand, GM-CSF was less detectable in the LI90 medium without the cytokine cocktail, suggesting that the cocktail induces expression of GM-CSF in LI90.

To identify the key cytokine involved in GM-CSF secretion from LI90 cells, we cultured LI90 cells in several combinations of FGF-1, FGF-2, LIF, SCF and HGF in the cytokine cocktail. When the LI90 cells were cultured with these 4 of the above-mentioned cytokines excluding FGF-2, GM-CSF secretion was markedly reduced similar to that when the cells were cultured without the cytokine cocktail (Fig. 4B). On the other hand, FGF-2 alone was sufficient to induce the secretion of considerable GM-CSF from LI90 cells (Fig. 4B). When UCB monocytes were cocultured with LI90 in the presence of FGF-2 alone (Fig. 4D), typical dendritic-shaped cells were observed as in addition of 5 cytokines (Fig. 4C). These results indicate that FGF-2 was the key factor responsible for GM-CSF secretion from LI90 cells, resulting in differentiation of monocytes into DCs in the LI90 coculture.

### Primary HSCs are capable of inducing DC differentiation from monocytes via GM-CSF expression

To address whether HSCs are involved in DC differentiation in the liver, we examined the potential of primary HSCs to DC differentiation from monocytes. We isolated HSCs isolated from normal rat liver and similarly cocultured with human UCB monocytes. After 7 days of coculture, typical dendritic-shaped cells were barely noted (Fig. 5A). In contrast, when monocytes were cocultured with HSCs isolated from $CCl_4$-treated rat liver, they differentiated into dendritic-shaped cells (Fig. 5B). In fact, these monocyte-derived cells strongly expressed DC-CK1, compared to coculture with quiescent HSCs from normal liver (Fig. 5C). GM-CSF expression was high in the cultured HSCs isolated from $CCl_4$-treated rat liver (activated rHSC, Fig. 5D). No expression of DC-CK1 was observed in freshly isolated UCB monocytes (see Day 0 in Fig. 2D). These results imply that activated HSCs, but not quiescent HSCs, are capable of inducing DC differentiation from monocytes via GM-CSF secretion.

## Discussion

In the present study, we show that HSCs induce differentiation of DCs from monocytes *in vitro*. The trans-well culture system enabled us to determine

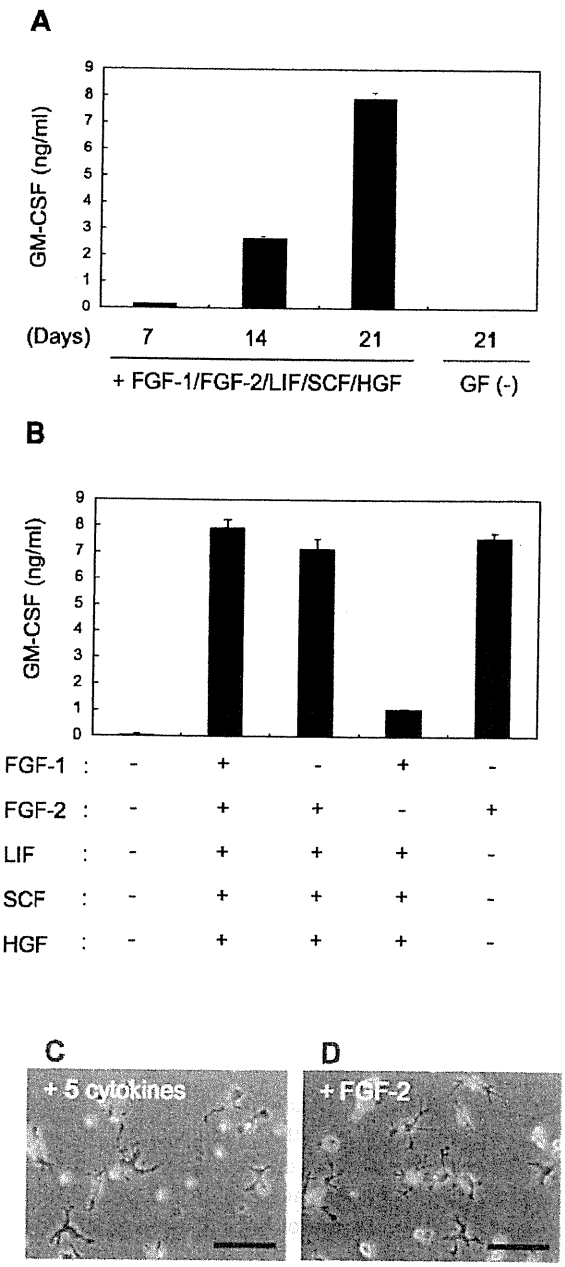


**Figure 4 : GM-CSF production of LI90 cells in the cytokine medium.** (A) The time course of GM-CSF production of LI90 cells ELISA was performed to detect GM-CSF in the LI90-cultured medium with or without FGF-1, FGF-2, LIF, SCF and HGF at the indicated days. GF (-), conditioned medium of LI90 cells without cytokines. (B) GM-CSF production of LI90 cells in culture with the indicated cytokines on Day 21. (C, D) Morphology of UCB monocytes cocultured with LI90 in the presence of 5 cytokines (C) or FGF-2 alone (D) for 21 days. Scale bars, 100 μm.

soluble factors from HSCs induce differentiation of monocytes to DCs. By addition of the cytokine cocktail, an HSC cell line LI90 increases the production of 7 cytokines more than 5-fold in culture. Among them, GM-CSF, IL-1$\beta$, IL-4 and IL-13 were of interest, because GM-CSF and IL-4 are known to contribute to the differentiation of DCs, and IL-1$\beta$ and IL-13 to their maturation.[13] It is known that GM-CSF induces DC differentiation *in vitro* from monocytes.[14] In addition, overexpression of GM-CSF in the liver results in an increase in the number of liver DCs.[15] Thus, we assume that increased secretion of GM-CSF from LI90 cells is responsible for DC differentiation from monocytes in the coculture. In fact, addition of anti-GM-CSF antibody to the LI90-conditioned medium prevented DC induction from monocytes, validating our assumption. The monocytes treated with the anti-GM-CSF neutralization antibody did not change their phenotypes and cell density, suggesting GM-CSF is not involved in survival of monocytes. We found that DCs induced by LI90 coculture from monocytes have a mature phenotype, because they exhibit a function of T cell activation. In DC differentiation *in vitro*, mature DCs are generally obtained in a 7-day culture of monocytes with GM-CSF and IL-4 followed by additional 2-day culture with maturation cytokines, such as IL-1$\beta$ and IL-13.[14] Since induction of GM-CSF production from LI90 is seen over 7 days after addition of FGF2 *in vitro*, we speculate that downstream signaling pathway(s), which are activated by FGF-2 signaling, indirectly participate in GM-CSF production in LI90.

Uwatoku et al.[16] reported that Kupffer cells can recruit DC precursors and DCs by direct binding to N-acetylgalactosamine-specific sugar receptors in the sinusoidal area. Furthermore, coculture of human monocytes with rat biliary epithelial cells or human non-parenchymal cells induces DC differentiation from monocytes.[17] However, it remains obscure whether HSCs are involved in DC differentiation. To examine a possible contribution of activated HSCs in an injured liver for the generation of DCs from monocytes, we cocultured monocytes with rat primary activated HSCs (Fig. 5). We found that activated HSCs isolated from $CCl_4$-treated rat liver markedly express GM-CSF and, thereby induce DC-CK1-expressing DCs extensively even in the xenogeneic coculture. Our results suggest that GM-CSF secreted from activated HSCs induces DC differentiation from monocytes in an injured liver.

Taking together previous reports and our present observations, we proposed a model of the generation of DCs from monocytes in an injured liver (Fig. 6). Upon

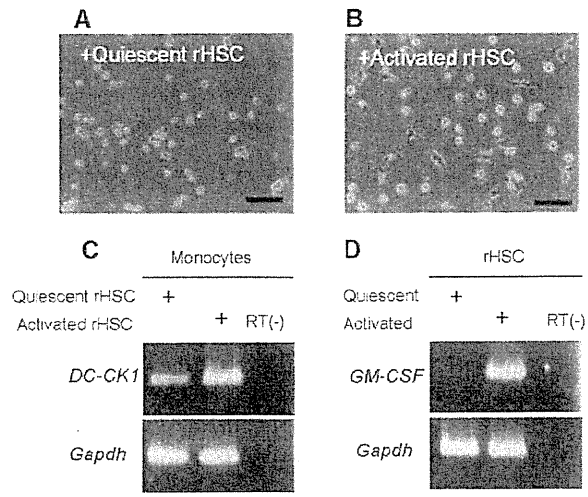


**Figure 5 : Coculture of UCB monocytes with HSCs from normal and $CCl_4$-treated rats.** (A, B) Morphology of UCB monocytes cocultured with HSCs from normal (A) or $CCl_4$-treated rat (B) in the cytokine medium for 7 days. Scale bars: 100 μm. (C) The gene expression of DC-CK1 in UCB monocytes cocultured with HSCs from normal (quiescent rHSC, lane 1) or $CCl_4$-treated rat (activated rHSC, lane 2) for 14 days. No amplification was detected in a negative control (activated rHSC, RT-) (D) The gene expression of GM-CSF in HSCs from normal (quiescent rHSC, lane 1) or $CCl_4$-treated rat (activated rHSC, lane 2) for 14 days under the coculture with UCB monocytes.

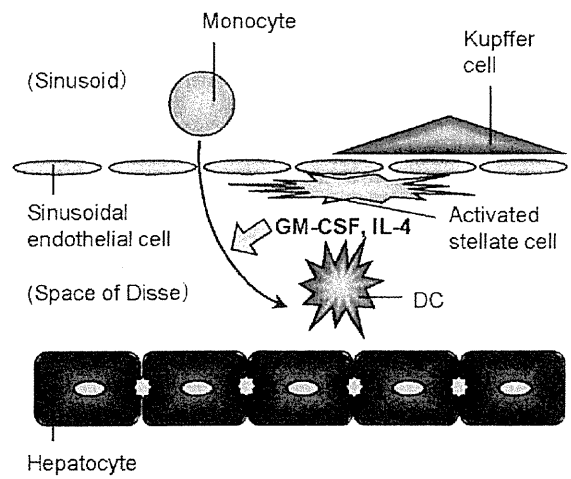


**Figure 6 : A proposed model for generation of DCs in the injured liver.** HSCs reside at the space of Disse in the sinusoids and in case of liver injury they are activated and release inflammatory cytokines including GM-CSF. Monocytes or dendritic precursor cells enter the space of Disse by cytokines released from several types of cells including activated HSCs. In the space of Disse, immature DCs are induced from monocytes or dendritic precursor cells by GM-CSF and IL-4 with subsequent maturation by other cytokines like IL-1$\beta$ and IL-13 released from activated HSCs. Mature DCs will migrate to lymph nodes via Glisson's sheath.

liver injury, HSCs in the space of Disse are activated and the activated HSCs consequently produce cytokines, including GM-CSF. These cytokines may attract monocytes or DC precursors into the space of Disse and contribute to monocyte differentiation into DCs. A histological analysis showed that DCs in the space of Disse are in direct contact with HSCs.[27] With regard to immune tolerance, Yu et al.[28] reported that activated HSCs suppress T-cell proliferation. Although the role of HSCs in hepatic immune responses is not fully understood,[18] HSCs may participate in the hepatic immune system via direct or indirect cellular interaction, including DC differentiation.

We identified that, among FGF-1, FGF-2, LIF, SCF and HGF in the cytokine cocktail, FGF-2 alone is sufficient to induce GM-CSF secretion in the human HSC line LI90, subsequently resulting in DC differentiation from monocytes in culture. Currently, 23 FGF genes have been identified in mice.[29] FGFs mediate a variety of cellular responses during organ development, injury, and regeneration. FGF signaling is mediated by binding FGF to FGF receptors (FGFRs), which belong to receptor tyrosine kinases. Four FGFRs have been identified and a variety of FGFR isoforms are known to be generated by alternative splicing of their transcripts. FGF-1 binds all known FGF receptors, whereas FGF-2 binds FGFR1b, FGFR1c, FGFR2c, FGFR3c, and FGFR4. FGF-1 and FGF-2 are expressed in a variety of tissues during both development and adulthood, but they are hardly expressed in normal liver. Induced FGF-2 expression has been known in HSCs during liver regeneration, and FGF-2 acts as a mitogen in autocrine and paracrine manners.[30,31] Gene knockout studies indicate that FGF-1 does not compensate the loss of FGF-2 in embryogenesis even though both FGF-1 and FGF-2 share the receptors.[32] It remains elusive how FGF-1 and FGF-2 differently affect cell responses. Heparan sulfate is known to modulate binding activities of those ligands to FGF receptors.[33] We found that activated HSCs isolated from $CCl_4$-treated rat liver markedly expressed GM-CSF (Fig. 5D). It seems that autocrine FGF-2 signaling in activated HSCs or paracrine effects of FGF-2 from other cells induce HSCs to secrete GM-CSF in the injured liver. Further studies will be necessary to address whether other cytokines are involved in FGF-2-mediated GM-CSF production in HSCs.

## Acknowledgements

This work was supported in part by Grants-in-Aid for Scientific Research (13470232, 16390357 and 18390343) from the Ministry of Education, Culture, Sports, Science and Technology, Japan. The authors declare no conflict of interest in this work. The authors thank Dr. K. Yasumizu (Kanto Medical Center NTT East Corporation, Tokyo, Japan) for supplying umbilical cord blood, Dr. T. Matsuura (The Jikei University School of Medicine, Tokyo, Japan) for providing the LI90 cell line, Dr. N. Kawada (Osaka City University) for preparing rat stellate cells and Dr. K. Nakahama (Tokyo Medical and Dental University) for supporting the neutralizing antibody experiment.

## Reference

1. Banchereau J, Steinman RM. Dendritic cells and the control of immunity. Nature 1998; 392: 245-52.
2. Longoni D, Piemonti L, Bernasconi S, et al. Interleukin-10 increases mannose receptor expression and endocytic activity in monocyte-derived dendritic cells. Int J Clin Lab Res 1998; 28: 162-9.
3. Inaba K, Inaba M, Romani N, et al. Generation of large numbers of dendritic cells from mouse bone marrow cultures supplemented with granulocyte/macrophage colony-stimulating factor. J Exp Med 1992; 176: 1693-702.
4. Sallusto F, Lanzavecchia A. Efficient presentation of soluble antigen by cultured human dendritic cells is maintained by granulocyte/macrophage colony-stimulating factor plus interleukin 4 and downregulated by tumor necrosis factor α. J Exp Med 1994; 179: 1109-18.
5. Rieser C, Böck G, Klocker H, et al. Prostaglandin E2 and tumor necrosis factor α cooperate to activate human dendritic cells: synergistic activation of interleukin 12 production. J Exp Med 1997; 186: 1603-8.
6. Muraille E, Trez CD, Pajak B, et al. T cell-dependent maturation of dendritic cells in response to bacterial super antigens. J Immunol 2002; 168: 4352-60.
7. Lau AH, Thomson AW. Dendritic cells and immune regulation in the liver. Gut 2003; 52: 307-14.
8. Crispe IN. Hepatic T cells and liver tolerance. Nat Rev Immunol 2003; 3: 51-62.
9. Kudo S, Matsuno K, Ezaki T, et al. A novel migration pathway for rat dendritic cells from the blood: hepatic sinusoids-lymph translocation. J Exp Med 1997; 185: 777-84.
10. Sato K, Nagayama H, Tadokoro K, et al. Interleukin-13 is involved in functional maturation of human peripheral blood monocyte-derived dendritic cells. Exp Hematol 1999; 27: 326-36.
11. Cabillic F, Rougier N, Basset C, et al. Hepatic environment elicits monocyte differentiation into a dendritic cell subset directing Th2 response. J Hepatol 2006; 44: 552-9.
12. Uwatoku R, Suematsu M, Ezaki T, et al. Kupffer cell-mediated recruitment of rat dendritic cells to the liver:

roles of N-acetylgalactosamine-specific sugar receptors. Gastroenterology 2001; 121: 1460-72.
13. Wake K. Perisinusoidal stellate cells (fat-storing cells, interstitial cells, lipocytes), their related structure in and around the liver sinusoids, and vitamin A-storing cells in extrahepatic organs. Int Rev Cytol 1980; 66: 303-53.
14. Asahina K, Sato H, Yamasaki C, et al. Pleiotrophin/heparin-binding growth-associated molecule as a mitogen of rat hepatocytes and its role in regeneration and development of liver. Am J Pathol 2002; 160: 2191-205.
15. Geerts A. History, heterogeneity, developmental biology, and functions of quiescent hepatic stellate cells. Semin Liver Dis 2001; 21: 311-35.
16. Bataller R, Brenner DA. Liver fibrosis. J Clin Invest 2005; 115: 209-18.
17. Pinzani M, Marra F. Cytokine receptors and signaling in hepatic stellate cells. Semin Liver Dis. 2001; 21: 397-416.
18. Winau F, Hegasy G, Weiskirchen R, et al. Ito cells are liver-resident antigen-presenting cells for activating T cell responses. Immunity 2007; 26: 117-29.
19. Kakinuma S, Tanaka Y, Chinzei R, et al. Human umbilical cord blood as a source of transplantable hepatic progenitor cells. Stem Cells 2003; 21: 217-27.
20. Tabata N, Ito M, Shimokata K, et al. Expression of fusion regulatory proteins (FRPs) on human peripheral blood monocytes: induction of homotypic cell aggregation and formation of multinucleatd giant cells by anti-FRP-1 monoclonal antibodies. J Immunol 1994; 153: 3256-66.
21. Murakami K, Abe T, Miyazawa M, et al. Establishment of a new human cell line, LI90, exhibiting characteristics of hepatic Ito (fat-storing) cells. Lab Invest 1995; 72: 731-9.
22. Sorg RV, Andres S, Kogler G, et al. Phenotypic and functional comparison of monocytes from cord blood and granulocyte colony-stimulating factor-mobilized apheresis products. Exp Hematol 2001; 29: 1289-94.
23. Wang YQ, Ikeda K, Ikebe T, et al. Inhibition of hepatic stellate cell proliferation and activation by the semisynthetic analogue of fumagillin TNP-470 in rats. Hepatology 2000; 32: 980-9.
24. Kawada N, Tran-Thi TA, Klein H, et al. The contraction of hepatic stellate (Ito) cells stimulated with vasoactive substances. Possible involvement of endothelin 1 and nitric oxide in the regulation of the sinusoidal tonus. Eur J Biochem 1993; 213: 815-23.
25. Kusano F, Tanaka Y, Marumo F, et al. Expression of C-C chemokines is associated with portal and periportal inflammation in the liver of patients with chronic hepatitis C. Lab Invest 2000; 80: 415-22.
26. Pillarisetty VG, Miller G, Shar AB, et al. GM-CSF expands dendritic cells and their progenitors in mouse liver. Hepatology 2003; 37: 641-52.
27. Sato T, Yamamoto H, Sasaki C, et al. Maturation of rat dendritic cells during intrahepatic translocation evaluated using monoclonal antibodies and electron microscopy. Cell Tissue Res 1998; 294: 503-14.
28. Yu M-C, Chen C-H, Liang X, et al. Inhibition of T-cell responses by hepatic stellate cells via B7-H1-mediated T-cell apoptosis in mice. Hepatology 2004; 40: 1312-21.
29. Eswarakumar VP, Lax I, Schlessinger J. Cellular signaling by fibroblast growth factor receptors. Cytokine Growth Factor Rev 2005; 16: 139-49.
30. Baruch Y, Shoshany G, Neufeld G, et al. Basic fibroblast growth factor is hepatotropic for rat liver in regeneration. J Hepatol 1995; 23: 328-32.
31. Hioki O, Minemura M, Shimizu Y, et al. Expression and localization of basic fibroblast growth factor (bFGF) in the repair process of rat liver injury. J Hepatol 1996; 24: 217-24.
32. Miller D, Ortega S, Bashayan O, et al. Compensation by fibroblast growth factor 1 (FGF1) dose not account for the mild phenotypic defects observed in FGF2 null mice. Mol Cell Biol 2000; 20: 2260-8.
33. Kan M, Wu X, Wang F, et al. Specificity for fibroblast growth factors determined by heparan sulfate in a binary complex with the receptor kinase. J Biol Chem 1999; 274: 15947-52.

OPEN ACCESS Freely available online

PLoS one

# Onset of Quiescence Following p53 Mediated Down-Regulation of H2AX in Normal Cells

**Yuko Atsumi[1☯], Hiroaki Fujimori[1,3☯], Hirokazu Fukuda[2☯], Aki Inase[2], Keitaro Shinohe[3], Yoshiko Yoshioka[3], Mima Shikanai[3], Yosuke Ichijima[3], Junya Unno[4], Shuki Mizutani[4], Naoto Tsuchiya[2], Yoshitaka Hippo[2], Hitoshi Nakagama[2], Mitsuko Masutani[1], Hirobumi Teraoka[3], Ken-ichi Yoshioka[1,3]***

1 Division of Genome Stability Research, National Cancer Center Research Institute, Tokyo, Japan, 2 Division of Cancer Development System, National Cancer Center Research Institute, Tokyo, Japan, 3 Department of Pathological Biochemistry, Medical Research Institute, Tokyo Medical and Dental University, Tokyo, Japan, 4 Department of Pediatrics and Developmental Biology, Graduate School of Medical and Dental Sciences, Tokyo Medical and Dental University, Tokyo, Japan

## Abstract

Normal cells, both *in vivo* and *in vitro*, become quiescent after serial cell proliferation. During this process, cells can develop immortality with genomic instability, although the mechanisms by which this is regulated are unclear. Here, we show that a growth-arrested cellular status is produced by the down-regulation of histone H2AX in normal cells. Normal mouse embryonic fibroblast cells preserve an H2AX diminished quiescent status through p53 regulation and stable-diploidy maintenance. However, such quiescence is abrogated under continuous growth stimulation, inducing DNA replication stress. Because DNA replication stress-associated lesions are cryptogenic and capable of mediating chromosome-bridge formation and cytokinesis failure, this results in tetraploidization. Arf/p53 module-mutation is induced during tetraploidization with the resulting H2AX recovery and immortality acquisition. Thus, although cellular homeostasis is preserved under quiescence with stable diploidy, tetraploidization induced under growth stimulation disrupts the homeostasis and triggers immortality acquisition.

**Citation:** Atsumi Y, Fujimori H, Fukuda H, Inase A, Shinohe K, et al. (2011) Onset of Quiescence Following p53 Mediated Down-Regulation of H2AX in Normal Cells. PLoS ONE 6(8): e23432. doi:10.1371/journal.pone.0023432

**Editor:** Michael Polymenis, Texas A&M University, United States of America

**Received** April 11, 2011; **Accepted** July 17, 2011; **Published** August 12, 2011



**Funding:** This study was supported by MEXT KAKENHI (20770136 and 20659047). The funders had no role in study design, data collection and analysis, decision to publish, or preparation of the manuscript.

**Competing Interests:** The authors have declared that no competing interests exist.

* E-mail: kyoshiok@ncc.go.jp

☯ These authors contributed equally to this work.

## Introduction

Cancer is a disease associated with genomic instability and the accumulation of mutations [1]. Unlike specific chromosomal translocation-associated tumors, most cancers associated with aging develop either chromosomal instability (CIN) or microsatellite instability (MIN) [2]. While MIN is associated with mismatch repair deficiency, CIN develops even in a normal background [3]. However, the mechanisms by which CIN and MIN develop remain elusive.

A recent genomic analysis of various cancers revealed that massive genomic rearrangements, including loss of heterozygosity (LOH) and chromosomal translocation, amplification and deletion, do not gradually accumulate over time, as conventionally thought, but appear to be acquired in a single catastrophic event [4]. One of such events could be associated with tetraploidization because tetraploidy is a common early event in cancer cells with CIN [5]. Tetraploidy is observed in cells during the initial stages of cancer [6,7] as well as in precancerous stages such as dysplasia [8,9], but not in malignant cancer cells, which usually exhibit aneuploidy in association with deploidization [5]. Furthermore, analogous to changes observed in cancer genomes, the immortalization of mouse embryonic fibroblasts (MEFs) occurs with tetraploidy and mutation of the Arf/p53 module, which eventually evolves into aneuploidy during serial cultivation [10].

In the initial stages of carcinogenesis, cells are subjected to oncogenic stress, resulting in the accumulation of DNA replication stress-associated lesions and the onset of barrier responses such as senescence and apoptosis [11,12]. This effect can be reproduced *in vitro* by the activation of oncogenes [11] and accelerated growth stimulation [12] due to the induction of accelerated S-phase entry and the resulting DNA replication stress. Importantly, genomic instability is generated under these conditions [11,12] because DNA replication stress-associated lesions persist into M phase and mediate chromosomal bridge formation and cytokinesis failure, resulting in tetraploidization [10]. In fact, tetraploidization of MEFs is induced via chromosomal bridge formation prior to the onset of immortality with mutation of Arf/p53 [10], although it is still unclear how tetraploidization induces immortality. Since such tetraploidization is specifically observed during senescence, tetraploidization might be a defect that occurs during cell proliferation or growth arrest. In fact, similar to cells in the initial stages of carcinogenesis, senescent cells often accumulate irreparable DNA lesions [13,14] and frequently exhibit genomic instability [15].

The development of cancer, as well as the onset of immortality in cells *in vitro*, is tightly associated with mutations in the Arf/p53 module [16–18]. Although this is ascribed to the role of p53 in

cancer prevention, the regulation and roles of p53 are complex [18]. While constitutively active p53 mediates premature aging in mice [19–21], additional single gene copies of *Arf* and *p53* under functional regulation mediate longevity and cancer prevention [22]. Similarly, while the accumulation of p53 induces cellular senescence and apoptosis [16,17], additional single gene copies of *Arf* and *p53* in MEFs has a protective effect from immortalization [22], suggesting that they help to maintain homeostasis under undamaged conditions. This raises the questions of the identity of the regulatory target of p53 in preserving cellular homeostasis under normal conditions and how cellular homeostasis preservation and abrogation are associated with genomic status and p53 regulation.

This study focused on the mechanism by which normal cells under serial proliferation regulate homeostasis preservation and abrogation and sought to identify the regulatory target of p53. Our results illustrated two distinct conditions that could result in growth-arrested cells: (i) cells that maintain continuous quiescence by down-regulating H2AX (a variant of core histone H2A) under p53 regulation and stable-diploidy maintenance; and (ii) cells that develop tetraploidy and immortality under continuous growth stimulation, characterized by the accumulation of γH2AX foci. Thus, oncogenic stress under growth stimulation triggers catastrophic tetraploidization that leads to immortalization in association with the accompanying mutation of the Arf/p53 module and recovery of H2AX expression and growth activity.

## Results

### Immortality is prevented in quiescent cells that maintain genomic stability

MEFs cultured under the standard 3T3 protocol (Std-3T3) senesce in association with oxygen sensitivity [23], which is followed by the development of immortality with tetraploidy [10] and mutation of the Arf/p53 module [22], similar to the process of carcinogenesis. In addition, similar to cells in the initial stages of carcinogenesis, spontaneous DNA lesions accumulate in senescent MEFs under Std-3T3 conditions prior to the development of immortality [10], which suggests that growth stimulation induced under Std-3T3 conditions might overwhelm senescent MEFs. Therefore, MEFs under Std-3T3 conditions were compared with MEFs exposed to temporary serum deprivation (tSD-3T3), which induces occasional growth arrest (Fig. 1A). Under Std-3T3 conditions, MEFs were immortalized with tetraploidy that progresses to aneuploidy (Fig. 1A–C). On the other hand, MEFs cultured under tSD-3T3 conditions never developed immortality and preserved quiescence with stable diploidy (Fig. 1A, C). This indicates that temporal growth arrest prevents immortalization and supports genomic stability. Conversely, continuous culture with 10% FBS produces oncogenic stress in senescent MEFs, triggering tetraploidization. Thus, even though both are growth arrested (at least in total cell numbers) with senescent morphology at the same culture passage (P9) (Fig. S1), MEFs under tSD-3T3 conditions are continuously quiescent with genomic stability, while MEFs under Std-3T3 conditions develop tetraploidy (Fig. 1A, C), posing a question in DNA lesion status that induces chromosomal bridge formation and tetraploidization [10].

### γH2AX foci accumulate in cells developing genomic instability but not in cells preserving diploidy

To determine the DNA lesion status induced by accelerated growth stimulation, γH2AX foci were compared in growth-arrested MEFs (P9) under both conditions (Fig. 1D). As expected, MEFs that developed tetraploidy under Std-3T3 conditions accumulated γH2AX foci, with some carrying over into the G2/M phases (Fig. 1E). This resulted in chromosome bridge formation (Fig. 1F) with the resulting tetraploidization that is initially observed with binucleated tetraploidy (Fig. 1F). On the other hand, quiescent MEFs that preserved genomic stability under tSD-3T3 conditions did not develop γH2AX foci (Fig. 1D), indicating that genomic stability is preserved under no γH2AX signal. However, it was still unclear why quiescent MEFs under tSD-3T3 conditions do not accumulate γH2AX foci because senescent cells are known to generally accumulate irreparable DNA lesions [13,14].

To address why γH2AX foci do not form under tSD-3T3 conditions, the expression level of H2AX at P9 was determined. As shown in Figure 1G, a remarkable reduction in H2AX expression was observed in quiescent MEFs at P9 while MEFs that developed tetraploidy under Std-3T3 conditions showed significantly higher H2AX expression than quiescent MEFs. This illustrates an association between H2AX levels and the cellular and genomic status, in that cells with largely diminished H2AX expression preserve stable diploidy and a quiescent status, while cells with residual H2AX expression and with γH2AX foci develop genomic instability and immortality (Fig. 1H). Importantly, H2AX-KO cells exhibited impaired DNA repair, growth retardation, and elevated genomic instability [24–28], phenotypes reminiscent of senescent cells. Therefore, it will be critical to determine how H2AX-status is regulated to produce quiescence and induce genomic instability.

### H2AX is generally diminished in quiescent cells

To address whether H2AX diminution is a general occurrence, H2AX expression was compared in normal human fibroblasts (NHFs) and MEFs. Decreased H2AX was observed in both cell types at growth-arrested stage after serial proliferation (Fig. 2A, B), suggesting that this process is conserved between humans and mice. In addition, H2AX diminution was also observed in many organs of adult mice, including the liver, spleen, and pancreas (Fig. 2C, D; Fig. S2). Thus, H2AX is generally reduced in quiescent cell chromosomes both *in vitro* and *in vivo*.

H2AX is also diminished during premature senescence induced by DNA damage. Using early passage MEFs (P2), H2AX diminution was observed when senescence was induced by treatment with hydroxyurea (HU) to induce DNA replication stress (Fig. 2E) and with the radiomimetic DNA-damaging agent, neocarzinostatin (Fig. S3). This most likely occurs because DNA repair is coupled with H2AX release and chromatin remodeling [29–31]. Together with results showing a decrease in H2AX transcript levels in senescent MEFs (Fig. S4), these results indicate that decreased amounts of H2AX protein in senescing cells is ascribed to a decrease in H2AX transcript levels and DNA damage.

To directly address the impact of H2AX reduction, H2AX was knocked down in early passage NHFs, which induced cellular quiescence with senescent cell characteristics; cells adopted a flattened and enlarged morphology and showed an increase in senescence-associated β-galactosidase activity (Fig. 2F). Since the knockdown of H2AX in 293T cells induced growth arrest without inducing a senescent morphology (data not shown), it is likely that the effect of H2AX diminution is primarily due to quiescence induction and potentially a normal consequence of senescence in normal cells.

### Immortalized cells develop following tetraploidization when H2AX status and growth activity are restored

The above results illustrate that cellular quiescence is produced when cells maintain stable diploidy and diminished H2AX

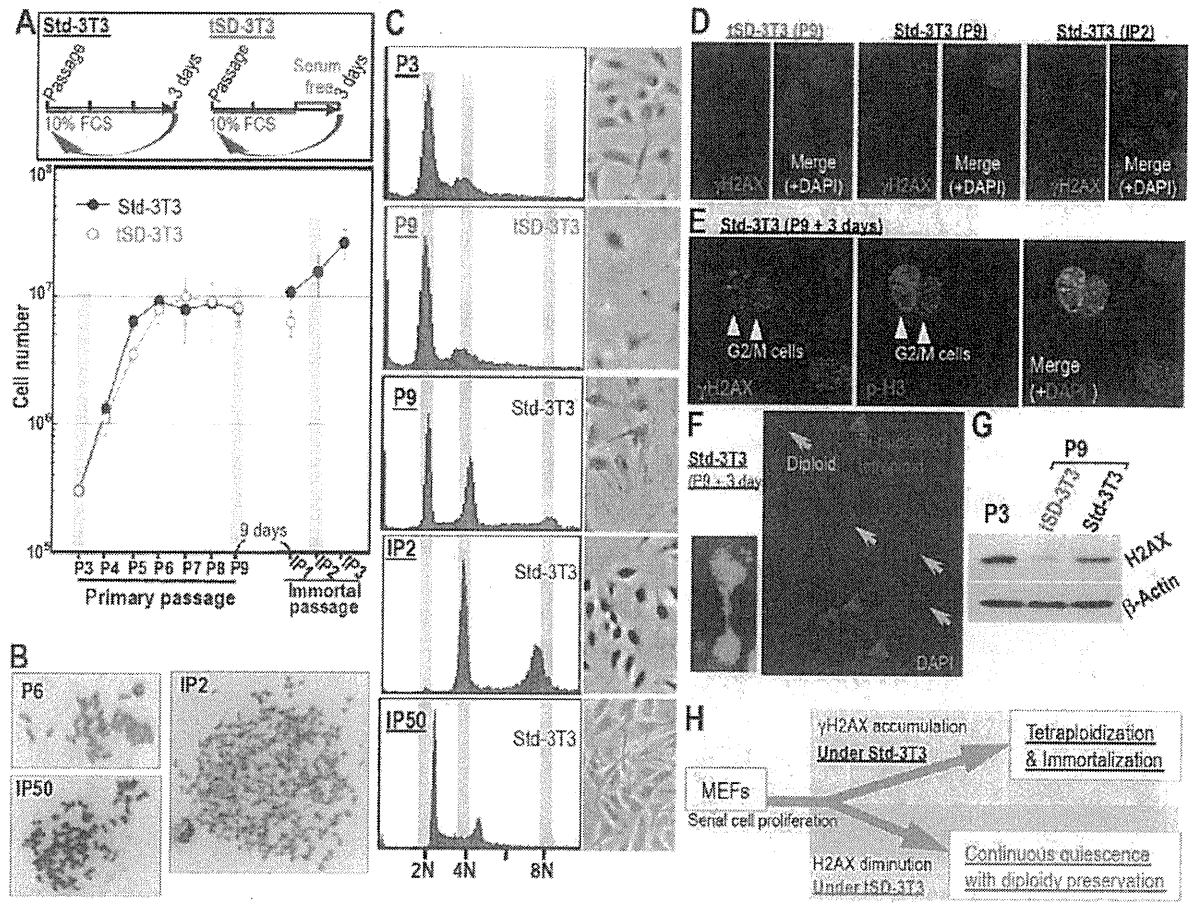


**Figure 1. Immortality with tetraploidy is blocked in quiescent cells with diploidy, diminished H2AX, and no γH2AX foci. A.** Growth curves of MEFs cultured under the standard 3T3 protocol (Std-3T3) or the T3 protocol with temporary serum deprivation (tSD-3T3) as schematically shown. MEFs under Std-3T3 conditions were immortalized, whereas MEFs cultured under tSD-3T3 conditions were not. **B** Genomic instability developed in immortalized MEFs (IP2) under Std-3T3 conditions. **C.** Genomic status was determined by flow-cytometry at the indicated conditions and passages. Representative images are shown. Tetraploidy development was blocked under tSD-3T3 conditions, while tetraploidy had already developed in growth-arrested MEFs at P9 under Std-3T3 conditions (see increasing 4N and 8N peaks). **D.** DNA lesions identified by γH2AX foci spontaneously accumulated in MEFs developing tetraploidy and immortality (P9) under Std-3T3 conditions as well as in immortal cells (IP2), while MEFs that maintained quiescent status with genomic stability under tSD-3T3 conditions contained no foci. **E.** DNA lesion-carryover into the G2-M phases was determined for lesions that spontaneously accumulated in senescent MEFs under Std-3T3 conditions. DNA lesions in senescing MEFs are also observed in the G2-M phases determined by phosphorylated H3. **F.** Chromosome bridge formation (Left panel) is observed in association with DNA lesion-carryover into the G2-M phases under Std-3T3 conditions with the resulting accumulation of bi-nucleated tetraploidy (Right panel: red arrow heads). Representative images are shown. **G.** The total H2AX level at P9 under each condition was determined. Whereas a significant reduction in H2AX expression was observed in MEFs with genomic stability under tSD-3T3 conditions, MEFs that developed immortality and genomic instability under Std-3T3 conditions did not show a significant decrease in H2AX expression. **H.** A model of the life-cycle of MEFs undergoing quiescence or developing immortality. While quiescent MEFs preserve diploidy and show diminished H2AX levels, MEFs developing immortality exhibited γH2AX foci accumulation.

doi:10.1371/journal.pone.0023432.g001

expression. In these cells, the H2AX level is less than 100-fold compared to that in actively growing cells. To study the effect of growth stimulation in cells with an H2AX-diminished quiescent status, complete medium (DMEM with 10% FBS) was added to quiescent MEFs prepared under tSD-3T3 conditions (Fig. 3A–C). In these cells, cell-cycle progression was initiated with the expression of PCNA and histones H3 and H2AX, which led to γH2AX foci formation (Fig. 3D, E). Abrogating quiescent status with complete medium resulted in the establishment of immortalized MEFs with tetraploidy (Fig. 3A–C). However, it took 30 days to initiate immortal passage in H2AX-diminished quiescent MEFs, while immortality was acquired in only 9 days for P9 MEFs under Std-3T3 conditions, suggesting that the H2AX-diminished quiescent status protected cells from immortalization. Supporting this argument, primary MEFs transfected with an H2AX expression vector also acquired immortality at an accelerated rate (Fig. S5A–C). Such H2AX-overexpression may induce the effect of DNA replication stress because immortality in H2AX-overexpressing MEFs were again developed with tetraploidy (Fig. S5D,E). Unexpectedly, H2AX status was totally recovered in actively growing, immortalized MEFs (Fig. 3F, G), which illustrates the association of H2AX status with growth activity.

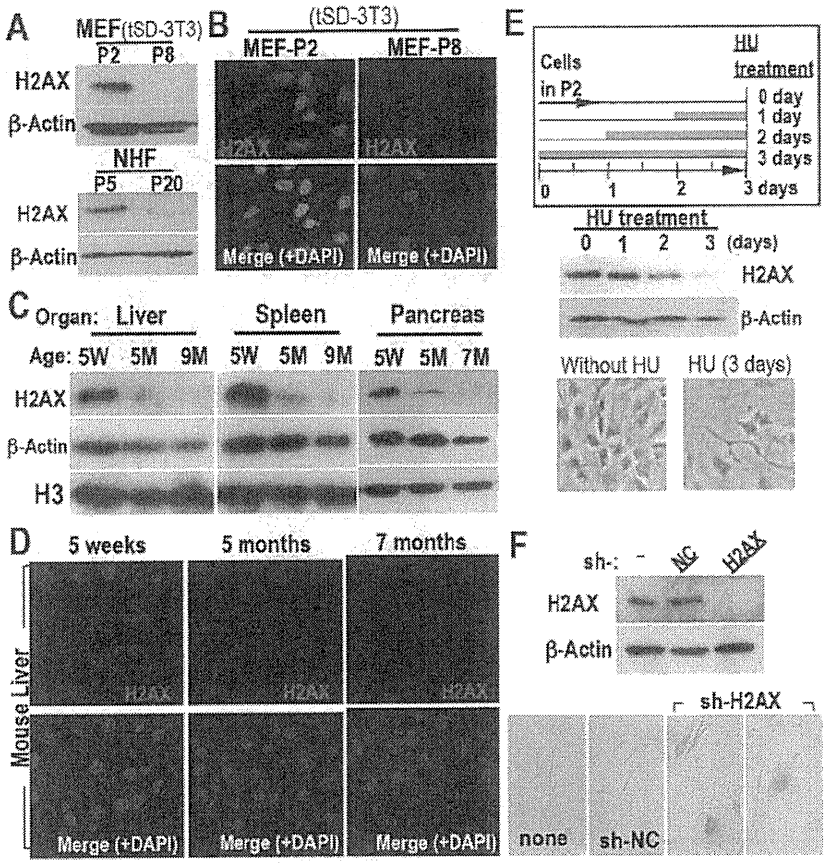


**Figure 2. Quiescent cell-status is induced with H2AX diminution both *in vitro* and *in vivo*.** **A,B** H2AX expression in growth-arrested cells (P8 for MEFs under tSD-3T3 conditions, P20 for NHFs) was determined by Western blotting (**A**) and immunofluorescent staining (**B**), revealing H2AX diminution in both types of growth-arrested cells. **C,D** H2AX diminution was also measured in adult mice organs by Western blotting (**C**) and in liver sections by immunofluorescent staining (**D**). Samples were prepared from five week (5W), five month (5M) and seven- or nine-month-old mice (7M or 9M). **E.** The involvement of H2AX diminution in DNA damage-induced premature senescence was determined after 0.2 mM HU treatment. Orange bars indicate the periods of HU treatment. Premature damage-induced senescence was observed with H2AX diminution, in which cells were flattened and enlarged, morphology typical of senescent cells. **F.** The effect of H2AX knockdown on senescence was determined in NHFs. Senescence was directly induced by H2AX knockdown in NHFs. H2AX status and senescence was determined by Western blotting (top) and SA-β-gal activation, and cells exhibited a flattened and enlarged morphology (bottoms), respectively.
doi:10.1371/journal.pone.0023432.g002

However, this also poses the question of how the down-regulation of H2AX expression in quiescent MEFs is reversed after immortalization.

## Immortalized cells no longer achieve H2AX diminution-associated quiescent status

To explore the effects of the change in H2AX status, the response of H2AX to DNA replication stress was compared between primary and immortalized MEFs. While H2AX in primary MEFs was down-regulated after HU treatment, this did not occur in immortalized MEFs (Fig. 3H), which indicates that H2AX diminution-associated quiescent cell status is not inducible after immortalization. Thus, quiescent status is preserved in cells with diminished H2AX expression and stable diploidy but is abrogated under continuous growth stimulation, inducing cell cycle progression and γH2AX foci formation, and eventually leading to immortality with tetraploidy and H2AX recovery. Since the Arf/p53 module is specifically mutated during MEF immortalization [22], p53 might be involved in H2AX down-regulation. In fact, unlike senescent normal cells, H2AX expression is relatively high (2–20% of total H2A) in cancer cells as well as in growing NHFs (10%) [28].

## H2AX diminution-associated quiescent status is produced by p53 and prohibits the development of immortality

To determine the involvement of p53 in H2AX down-regulation, *p53* knockout (KO) MEFs were cultured. Unlike normal primary MEFs, but similar to immortalized MEFs (Fig. 3H), H2AX expression in primary *p53*-KO-MEFs was not decreased by HU treatment (Fig. 4A). Furthermore, *p53*-KO-MEFs continuously grew, without change in H2AX status even under tSD-3T3 conditions (Fig. 4B, C). This indicates that H2AX in wild-type (WT)-MEFs is down-regulated by p53 to

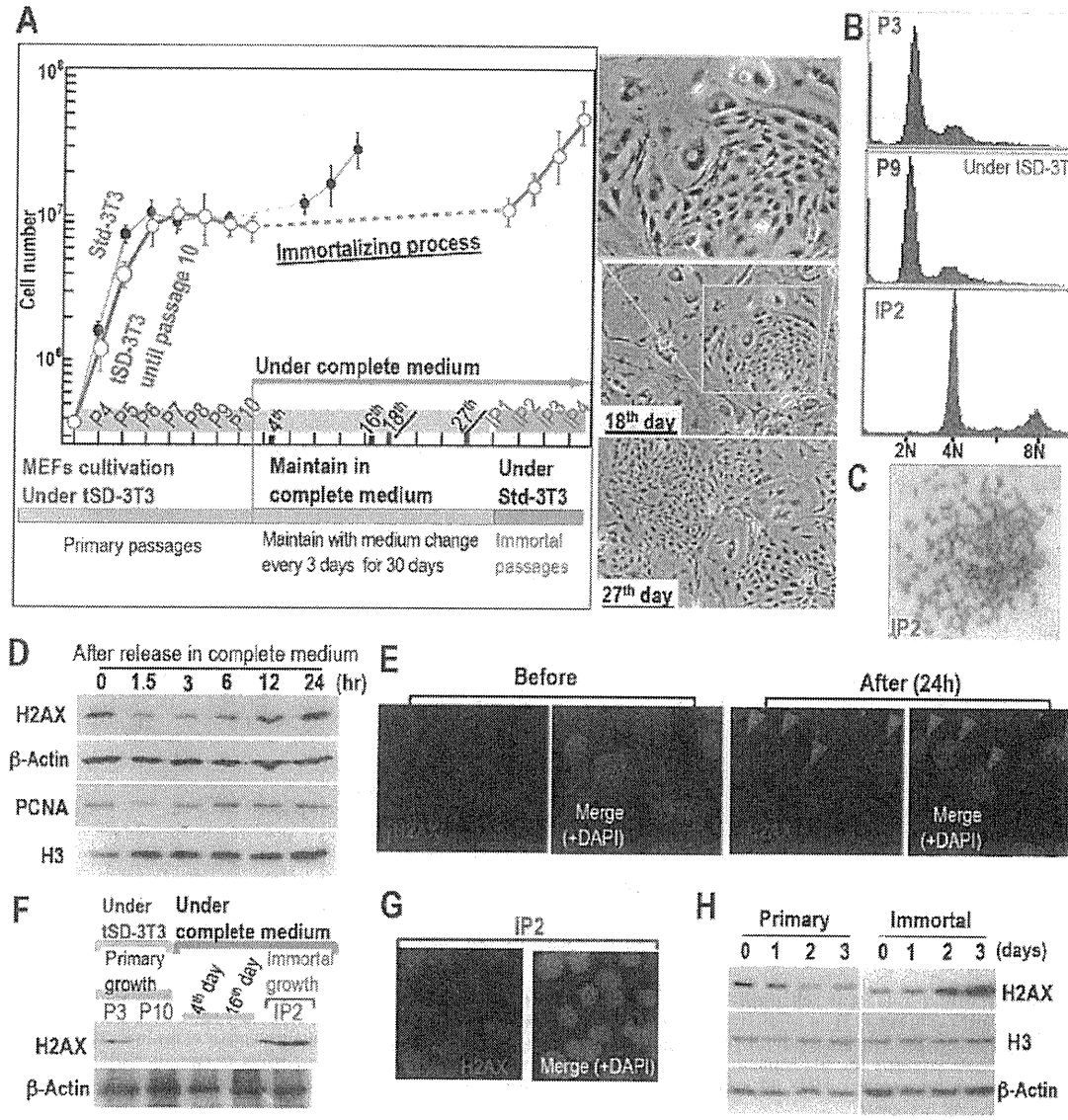


**Figure 3. H2AX-diminished quiescent cell-status is abolished by continuous growth stimulation with accompanying H2AX recovery. A.** Quiescent MEFs with diminished H2AX expression were cultured under tSD-3T3 conditions until P10. They were then exposed to complete medium, which was changed every three days for 30 days. Immortal passages were started under Std-3T3 conditions (red circles). MEFs cultured under the Std-3T3 conditions (black circles) as in Figure 1a were superimposed for comparison of the time needed to acquire immortality. Representative images of MEFs during the process of acquiring immortality are also shown. **B,C.** Tetraploidy development in immortalized MEFs (IP2) was observed by flow-cytometry (**B**) and Giemsa staining (**C**). **D.** Growth acceleration-associated cell cycle progression and H2AX induction. To determine the effect of serum induction on H2AX expression and cell cycle progression, senescent MEFs at P8 were incubated in serum-free medium for 24 h and harvested after exposure to complete medium for various times. H2AX expression increased with increasing PCNA and histone H3, which suggests that the expression of these chromatin factors was associated with S phase entry. To detect H2AX levels in these MEFs at P8, the H2AX signal was visualized by longer exposure. **E.** DNA lesions characterized by γH2AX foci were induced in MEFs (red arrowheads) after exposure to complete medium as in **D**. **F,G.** H2AX status in immortalized MEFs was determined by Western blotting (**F**) and immunofluorescence (**G**), revealing H2AX recovery. **H.** DNA replication stress-associated H2AX diminution was compared between normal and immortalized MEFs as in Figure 2E, in which H2AX was not down-regulated after immortalization.
doi:10.1371/journal.pone.0023432.g003

induce cellular quiescence and is recovered in immortalized MEFs in association with tetraploidization and mutation of the Arf/p53 module. Although *p53*-KO-MEFs did not undergo H2AX diminution-mediated growth arrest, these MEFs still exhibited a senescent morphology (Fig. 4D, see P8) and subsequently achieved an immortalized morphology (P14), which suggests the immortalization of *p53*-KO-MEFs via the senescent stage without growth arrest. This also indicates that a quiescent cell status is induced by p53 to protect cells from immortality.

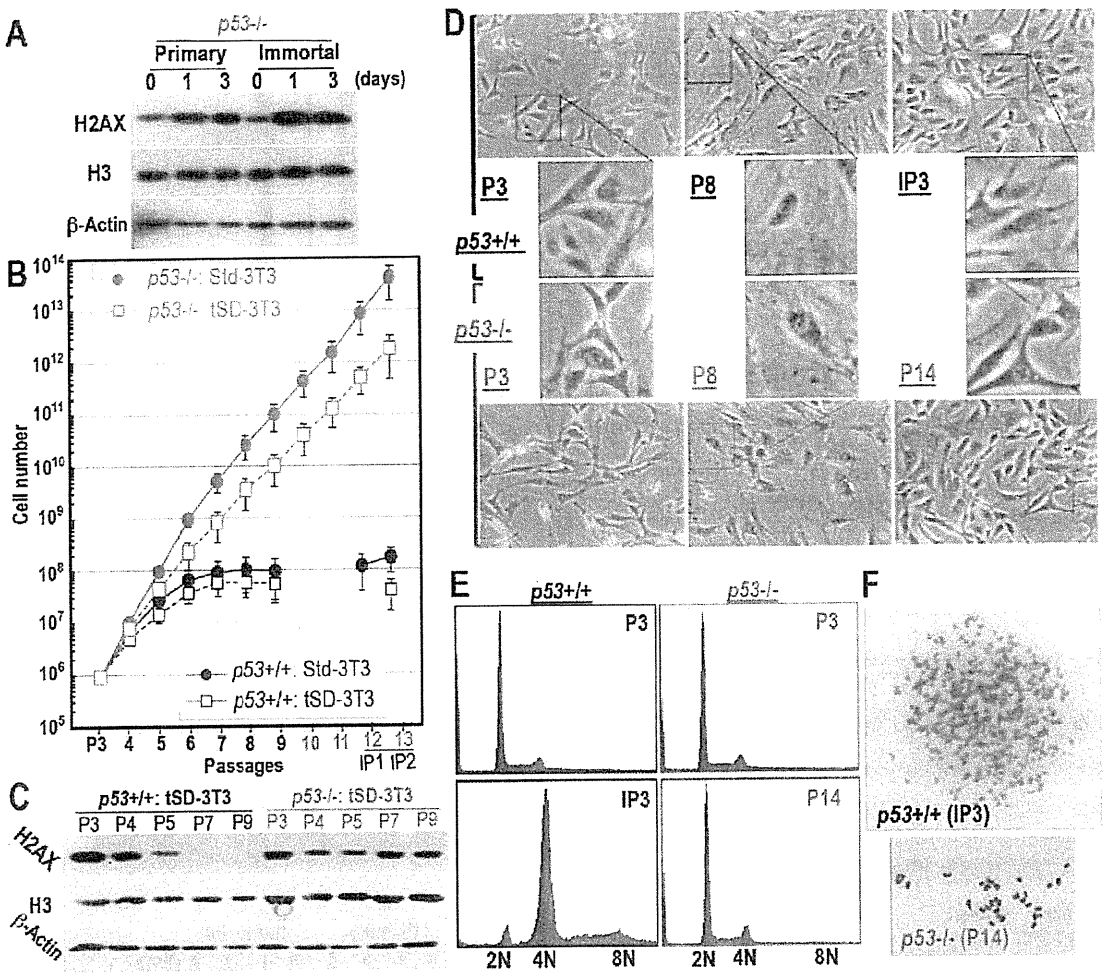


**Figure 4. H2AX-diminished quiescent cell status is regulated by p53. A.** DNA replication stress-associated H2AX diminution status was determined in *p53*-KO MEFs as in Figure 2E, in which H2AX was not down-regulated, even in primary MEFs. **B–F.** Primary *p53*-KO MEFs were cultured during the senescing and immortalizing processes (**B**). H2AX status was determined by Western blotting (**C**), morphological assessment (**D**), genomic status determined by flow-cytometry (**E**), and chromosome spread (**F**). Although *p53*-KO MEFs never showed major changes in H2AX expression, tetraploidization or growth arrest, *p53*-KO MEFs still exhibited a senescent morphology (P8) before achieving an immortalized morphology (P14).
doi:10.1371/journal.pone.0023432.g004

## Mutation of the Arf/p53 module is induced with tetraploidization, triggered by DNA replication stress under moderately decreased H2AX levels in normal cells

Whereas *p53*-KO-MEFs are immortalized with diploidy (Fig. 4E, F), WT-MEFs are never immortalized only after tetraploidization [10] (Fig. 1B, C; Fig. 3B, C; Fig. 4E, F) and loss of Arf/p53 [22]. This suggests that the mutation of the Arf/p53 module in WT-MEFs is induced during tetraploidization. Supporting this argument, p53-dependent quiescence produced by diminished H2AX is maintained under diploidy preservation but abrogated after tetraploidization with mutation in the Arf/p53 module and the resulting H2AX recovery (Fig. 3). Therefore, normal WT-MEFs are protected from immortalization by a quiescent cell status, as long as the genome is preserved in diploidy. However, under continuous growth stimulation, tetraploidization also spontaneously arises in WT-MEFs but, unexpectedly, not in *p53*-KO-MEFs.

As tetraploidization was observed at the senescent stage under conditions of continuous growth stimulation that induce DNA replication stress (Fig. 3), the underlying reason for tetraploidization in WT-MEFs but not in *p53*-KO-MEFs might be associated with the repair deficiency that also occurs in an H2AX-diminished background. To examine the tetraploidization risk under an H2AX-diminished background, MEFs of each type were treated with HU for 36 hours and the incidence of bi-nucleated tetraploidy formation was compared (Fig. 5A). As expected, HU treatment-associated H2AX diminution (Fig. 2E) resulted in tetraploidization in primary WT-MEFs but not in immortalized WT-MEFs or p53-KO-MEFs (Fig. 5A). Thus, although normal cells become quiescent with largely diminished H2AX under diploidy, senescing cells with residual H2AX under growth stimulating conditions are potentially at risk of developing tetraploidy in response to DNA replication stress.

Finally, to address changes in DNA replication stress-sensitivity during serial proliferation of normal MEFs, the repair efficiencies

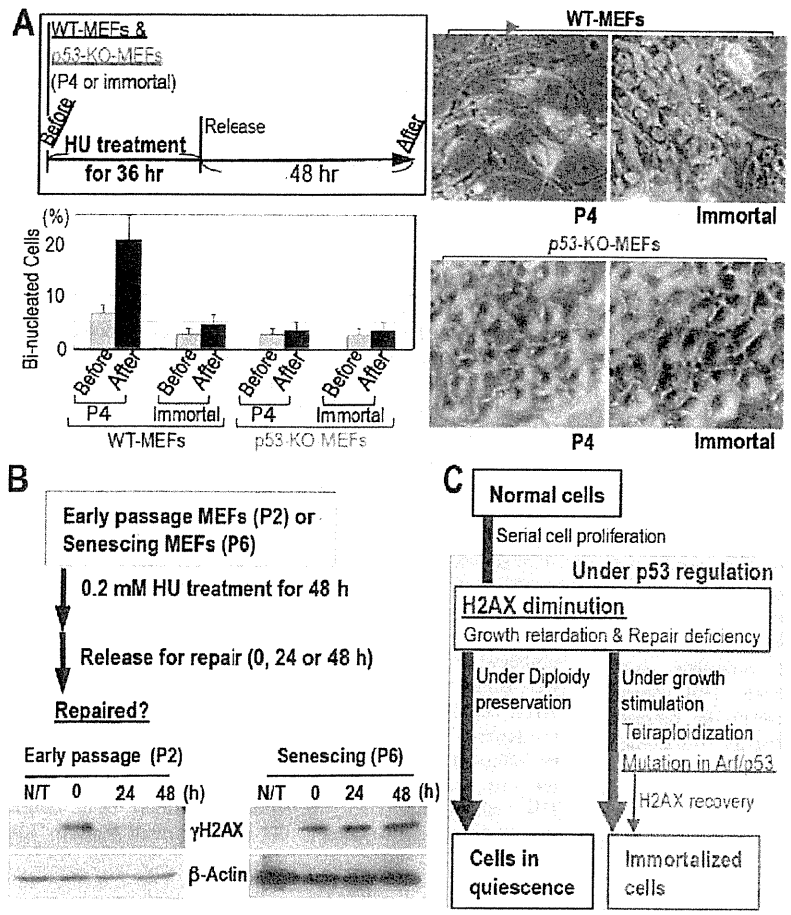


**Figure 5. Increased risk of tetraploidization in normal MEFs. A.** DNA replication stress-associated tetraploidization was determined in MEFs (P4) with the formation of bi-nucleated tetraploidy (red arrowhead) after 0.2 mM HU treatment as illustrated (top-left panel). Tetraploidization was efficiently induced during primary growth but not in immortalized MEFs or *p53*-KO-MEFs. **B.** Repair efficiencies of DNA replication stress-associated lesions were compared between early passage (P2) and senescing MEFs (P6) after 48 h hydroxyurea (HU) treatment. γH2AX signal was used as a marker of DNA lesions, in which γH2AX signal and β-Actin signals in senescing MEFs (P6) were detected only with over-exposure compared to early passage MEFs (P2), due to decreased H2AX levels during senescence. The reduction in γH2AX signal after release was only evident in early passage MEFs, which suggests that senescing cells are defective in resolving DNA replication stress. **C.** A model of MEFs under serial cell proliferation either undergoing quiescence or developing immortality. While MEFs that maintain quiescence and diploidy show diminished H2AX levels, MEFs developing immortality accumulate γH2AX foci.
doi:10.1371/journal.pone.0023432.g005

of DNA replication stress-associated lesions were compared between early passage and senescent MEFs with the decay of the γH2AX signal after release from HU treatment (Fig. 5B). Unlike early passage MEFs (P2), senescing MEFs (P6) were deficient in repairing HU-associated DNA lesions (Fig. 5B), in which MEFs show slow cell-cycle progression and residual H2AX expression. This is in contrast to quiescent MEFs with largely diminished H2AX level that show neither detectable cell cycle progression nor DNA replication stress. Thus, normal cells under serial proliferation decrease H2AX expression; thereby, cells slow growth activity and become defective in DNA repair. In such cells, cellular homeostasis is preserved by quiescence under largely diminished H2AX level regulated by p53 as long as diploidy is preserved. However, these cells are simultaneously at increased risk of tetraploidization with p53 dysfunction under continuous growth acceleration, resulting in the development of immortality and recovery of H2AX activity and cell growth (Fig. 5C).

## Discussion

The results of this study revealed the following novel concepts: (i) normal cells generally achieve quiescent status with diminished H2AX level both *in vitro* and *in vivo*, and this is regulated by p53; (ii) growth arrested normal cells with senescent morphology can be defined as either (a) those in a continuous quiescent status with largely diminished H2AX level or (b) those in a transient status with inducing genomic instability and the resulting onset of immortality, under which cells accumulate γH2AX foci; (iii) to protect cells from immortality, one of the critical roles of p53 is the induction of growth-arrest via the down-regulation of H2AX with cellular quiescence. Cells in H2AX diminution-associated quiescence are shown in the cause of mature and premature senescence, during which cells show senescent morphology (Fig. S1), probably because these cells are repair defective (Fig. 5B). However such repair deficiency is also associated with genomic instability

development under accelerated growth stimulation, resulting in immortality acquisition with Arf/p53 module mutation and H2AX recovery.

Since growth-arrested cellular status with senescent morphology is directly induced by H2AX-knockdown (Fig. 2F), H2AX down-regulation is involved in a cause of quiescent cellular status. On the other hand, residual H2AX-expression in senescent cells is an associated effect for tetraploidization and immortalization: residual H2AX in senescent cells are only observed under accelerated growth stimulation (Figs. 1 and 3), under which cells are subjected to DNA replication stress and exhibit γH2AX, resulting in tetraploidization. Thus, even though cells are morphologically senescent with no growth in total cell number, cellular statuses could be either cells developing genomic instability under continuous growth acceleration (Std-3T3) or continuously quiescent cells under occasional arrest (tSD-3T3).

Unlike highly accumulated p53 that induces apoptosis, the Arf/p53 module under normal conditions functions for longevity by suppressing tumors in mice and giving protection from immortalization in MEFs [22]. Here, our results illustrated that such cellular status is produced with H2AX diminution-associated quiescence by protecting from immortalization under normal p53 regulation but is abrogated by Arf/p53 module mutation that is induced with tetraploidization under continuous growth stimulation, resulting in recovery of H2AX and growth activity. Unlike cells undergoing apoptosis, cells preserving quiescence under normal conditions do not accumulate p53 protein [10], which is probably associated with p53 function expression for quiescent status preservation but not for apoptosis induction. Intriguingly, such p53-dependent H2AX diminution was only observed after cells reach growth arrest both *in vivo* and *in vitro* but not growing cells in early passages and in organs from young mice (Fig. 2). In accordance with this, the expression of p53 targets Sidt2 and Phlda3, which are likely associated with tumor suppression [32], were elevated after cells become H2AX diminution-associated quiescent (P7) compared to cells in early passage (P3) (Fig. S6). However, similar to p53 protein, the increase in p53 transcript is also limited (Fig. S6). Thus, p53 function is expressed for apoptosis with accumulated p53, otherwise for H2AX-diminution associated quiescent status preservation under normal regulation without accumulating p53.

Except for tumors associated with specific chromosomal translocation, development of most cancers as well as *in vitro* cellular transformation is associated with genomic instability of either CIN or MIN [2,3]. Importantly, tetraploidization, a major initial form of CIN under a mismatch repair proficient background is induced with oncogenic stress by accelerated S-phase entry [10], leading to immortality acquisition in MEFs with mutation in the Arf/p53 module. Here, our results showed that quiescence could be preserved with largely diminished H2AX and diploidy preservation under the regulation of p53. Although H2AX down-regulation is only observed under functional p53 regulation, it is still unclear how p53 down-regulates H2AX. Our results showed the reduction of total H2AX transcript during the senescing process (Fig. S4) and a damage-induced decrease of H2AX protein under functional p53 regulation (Fig. 2E; Fig. 4A, B). Although p53 role for H2AX down-regulation is unclear, the regulation might be indirect because (1) there is no p53-binding site on the *H2AX* promoter, (2) there is no signal of the *H2AX* gene with ChIP-on-CHIP analyses against p53 [33], (3) H2AX expression does not associate with the activation level of p53 as we observed no association between H2AX expression and p53 activation (Fig. S7).

Together, our results provide a rationale for the regulation of cellular homeostasis preservation. By prohibiting immortality development and preserving quiescent cell status, p53 induces an H2AX diminution-mediated quiescent status. However, this status is abrogated by continuous growth stimulation, which results in the induction of genomic instability with mutation of the Arf/p53 module, which leads into H2AX recovery, the restoration of growth activity, and immortality acquisition (Fig. 5C).

## Methods

### Ethics Statement

Mice were treated in accordance with the Japanese Laws and the Guidelines for Animal Experimentation of National Cancer Center. All experiments were approved by The Committee for Ethics in Animal Experimentation of National Cancer Center (approval ID numbers: A59-09 and T07-038).

### Cell culture and tissue samples

Cells were cultured as described previously [34]. Both wild-type and *p53*-KO MEFs were prepared from day 13.5 embryos of wild type and $p53^{(+/-)}$ mice [35] as previously described [34] and cultured under the standard 3T3 (Std-3T3) passage protocol [36] or with the following modifications: tSD-3T3. Senescing MEFs (P6 or P8) were maintained under tSD-3T3 conditions for the experiments shown in Figures 2, 3, 4, 5. NHFs (normal human umbilical cord fibroblasts; HUC-F2, RIKEN BRL Cell Bank) were cultured under Std-3T3 conditions. Resveratrol treatment of NHFs was performed as for MEFs. For the H2AX shRNA study, the reported sequence oligonucleotide [37,38] was inserted into the pSuper.retro.puro vector (Oligoengine) and the shRNA virus was then prepared using 293T cells. The virus was infected into NHF cells and selected with puromycin. Mouse tissue samples were prepared from mice at the ages indicated (Sankyo Labo Service).

### DNA damage and induction of replication stress

DSB damage was induced by neocarzinostatin (Pola Pharma, Tokyo, Japan) treatment. For induction of DNA replication stress, MEFs were treated with hydroxyurea (HU).

### Antibodies, immunostaining and Western blotting

Antibodies against γH2AX (JBW301, Upstate Biotechnology) and H2AX (Bethyl) were used for immunostaining and Western blot analysis. Antibodies against β-actin (AC-74, Sigma), PCNA (Santa Cruz) and histone H3 (ab1791, Abcam) were used for Western blot analysis. Prior to immunostaining with primary and secondary antibodies, cells were fixed with 4% paraformaldehyde for 10 min and permeabilized with 0.1% Triton X-100/PBS for 10 min. Western blot analysis and confocal microscopy were performed as described previously [10].

### Transcription level analyses with RT-PCR

Total RNA was extracted from MEFs with the RNeasy system (Sigma). RNA (0.8 μg) was reverse-transcribed using a cDNA Archive kit (Applied Biosystems) and subjected to PCR. The following PCR primers were used: H2axf, 5′-TTGCTTC-AGCTTGGTGCTTAG-3′; H2axr, AACTGGTATGAGGC-CAGCAAC; β-actinf, CATCCAGGCTGTGCTGTCCCTGTA-TGC; and β-actinr, GATCTTCATGGTGCTAGGAGCCA-GAGC; Trp53-F, CGGATAGTATTTCACCCTCAAGATC-CG; Trp53-R, AGCCCTGCTGTCTCCAGACTC; Sidt2-F, CGGAAGGCTGGTTTCTGAGTTTCCG; Sidt2-R, CTGTA-AACGCCAAGGACCAGAA; Phlda3-F, CGGTCCATCTAC-